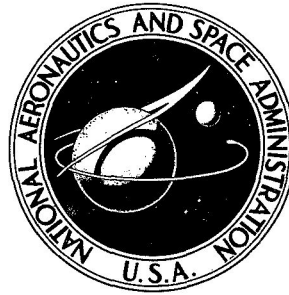


N70-32853

NASA TECHNICAL NOTE

NASA TN D-5891



NASA TN D-5891

CASE FILE COPY

1000-HOUR ENDURANCE TEST OF A GLASS-COATED ACCELERATOR GRID ON A 15-CENTIMETER-DIAMETER KAUFMAN THRUSTER

by Bruce A. Banks and Robert T. Bechtel

Lewis Research Center
Cleveland, Ohio 44135



1. Report No. NASA TN D-5891	2. Government Accession No.	3. Recipient's Catalog No.	
4. Title and Subtitle 1000-HOUR ENDURANCE TEST OF A GLASS-COATED ACCELERATOR GRID ON A 15- CENTIMETER-DIAMETER KAUFMAN THRUSTER		5. Report Date July 1970	6. Performing Organization Code
		8. Performing Organization Report No. E-5393	
7. Author(s) Bruce A. Banks and Robert T. Bechtel		10. Work Unit No. 120-26	11. Contract or Grant No.
9. Performing Organization Name and Address Lewis Research Center National Aeronautics and Space Administration Cleveland, Ohio 44135		13. Type of Report and Period Covered Technical Note	
		14. Sponsoring Agency Code	
12. Sponsoring Agency Name and Address National Aeronautics and Space Administration Washington, D. C. 20546			
15. Supplementary Notes			
16. Abstract A dished, glass (Corning 7052)-coated, molybdenum, accelerator grid was operated for 1000 hr on a 15-cm-diameter Kaufman mercury thruster. Grid lifetime estimates based on grid weight loss, glass erosion, and molybdenum erosion were made after 508 hr of operation at an average net accelerating potential of 990 V and at an average ion beam current of 373 mA. Grid-edge-termination schemes tested during the last 492 hr of the test indicate that the outermost holes and edge of the grid should be shadow shielded from the discharge chamber plasma and sputtered material.			
17. Key Words (Suggested by Author(s)) Composite Ion Glass-coated Thruster Accelerator grid Electron bombardment		18. Distribution Statement Unclassified - unlimited	
19. Security Classif. (of this report) Unclassified	20. Security Classif. (of this page) Unclassified	21. No. of Pages 48	22. Price* \$3.00

*For sale by the Clearinghouse for Federal Scientific and Technical Information
Springfield, Virginia 22151

CONTENTS

	Page
<u>SUMMARY</u>	1
<u>INTRODUCTION</u>	2
<u>APPARATUS AND PROCEDURE</u>	2
FACILITY	2
THRUSTER	3
ACCELERATOR GRID	4
Initial Geometry	4
Mounting System	9
NEUTRALIZER	9
Geometry	9
Operation	9
CONTROL LOGIC	11
UNATTENDED THRUSTER OPERATION	14
<u>RESULTS AND DISCUSSION</u>	15
FIRST 508 HOURS OF TEST	21
Accelerator-Grid Drain Current	21
Primary ion impingement	21
Surface conductivity of sputtered material	24
Electrical volume conductivity of glass coating	24
Charge-exchange ion impingement	25
Accelerator-Grid Lifetime Estimates	26
Weight loss	26
Glass erosion	29
Molybdenum erosion	29
LAST 492 HOURS OF TEST - GRID-EDGE-TERMINATION STUDIES	30

	Page
<u>SUMMARY OF RESULTS</u>	38
 <u>APPENDIXES</u>	
<u>A - SYMBOLS</u>	40
<u>B - EFFECT OF BREAKDOWN SITE LOCATION ON GRID DURABILITY</u>	41
 <u>REFERENCES</u>	 45

1000-HOUR ENDURANCE TEST OF A GLASS-COATED ACCELERATOR GRID ON A 15-CENTIMETER-DIAMETER KAUFMAN THRUSTER

by Bruce A. Banks and Robert T. Bechtel

Lewis Research Center

SUMMARY

A glass-coated molybdenum accelerator grid was operated on a 15-centimeter-diameter Kaufman mercury thruster for 1000 hours. The grid consisted of a 0.525-millimeter-thick Corning glass (code 7052) coating on a 0.38-millimeter-thick perforated molybdenum sheet having 1.9-millimeter-diameter holes arranged in a 51-percent-open-area hexagonal array. The 1000-hour endurance test was divided into two main testing periods. The first segment was a 508-hour test to provide durability, performance, and lifetime information about the grid. The results of this test indicated that if an appropriate grid-edge-termination scheme could be devised, expected lifetimes ranged from 22 000 to 37 000 hours, depending on the mode of grid failure. During this segment of the test, the grid was operated at the following average operating conditions:

- (1) 990 Volts net accelerating potential
- (2) -456 Volts accelerator potential
- (3) 373 Milliamperes mercury ion beam current
- (4) 9.4 Milliamperes accelerator drain current
- (5) Greater than 90-percent propellant utilization efficiency

Numerous electrical breakdown sites observed at the outermost grid holes during the initial 508 hours resulted in ion sputtering damage to the molybdenum in the area of these breakdown sites.

The final 492-hour segment of the 1000-hour test consisted of a series of tests of four grid-edge-termination modifications designed to prevent electrical breakdown and grid degradation. The results of the edge-termination tests indicated that shadow shielding of the outer edge of the grid successfully eliminated these problems. In addition, after a total of 1000 hours operating time, the grid had no observable erosion pattern associated with neutralizer efflux, or any other degradation which would have prevented further operation of the grid.

INTRODUCTION

Tests of composite accelerator grids on Kaufman thrusters have indicated that substantial performance gains over conventional double-grid systems may be possible (refs. 1 to 3). For example, the use of composite accelerator grids permits thruster operation at specific impulses of about 2000 seconds with ion production losses approximately one-half those resulting from double-grid systems. Numerous tests of Corning 7052 glass-coated accelerator grids have indicated very acceptable performance at net accelerating potentials of 1000 volts or less (refs. 3 and 4). These tests, however, were of relatively short duration (<100 hr) and provided little information on the long-term characteristics of glass-coated accelerator grids. Grid durability in excess of 10 000 hours may be required for some applications.

A 1000-hour endurance test of a dished glass-coated accelerator grid on a 15-centimeter-diameter mercury Kaufman thruster was undertaken to provide data on the durability of this type of grid. A detailed inspection of the grid after 500 hours of operation was scheduled to identify any degradation factors or modes of failure which might lead to short grid lifetimes. The results of this inspection and analysis of the grid performance would be used to provide guidelines for design modifications, if necessary, that would be evaluated during the second 500-hour test period.

This report presents the results of the 1000-hour test. The equipment used in the experiment is described first. The results of the initial 508-hour test are then presented and discussed. Degradation factors and estimated lifetime are considered. The modifications and performance obtained during the final 492 hours of testing are then described. Symbols are defined in appendix A, and details of electrical breakdown phenomena encountered during testing are considered in appendix B.

APPARATUS AND PROCEDURE

FACILITY

The tests described herein were performed in a vacuum tank 7.6 meters in diameter by 20 meters long (ref. 5). The tank is pumped by twenty 0.8-meter-diameter oil diffusion pumps, and associated equipment. The thruster was mounted in a 0.9-meter-diameter bell-jar chamber separated from the tank by a 1-meter gate valve (see fig. 1). This permitted removal of the thruster without opening the main tank. The thruster was mounted on a translatable framework. The thruster was moved into the tank about 0.3 meter from the retracted position after the bell jar had been pumped down and the gate valve opened. In the extended position the ion beam did not strike the walls of the bell jar.

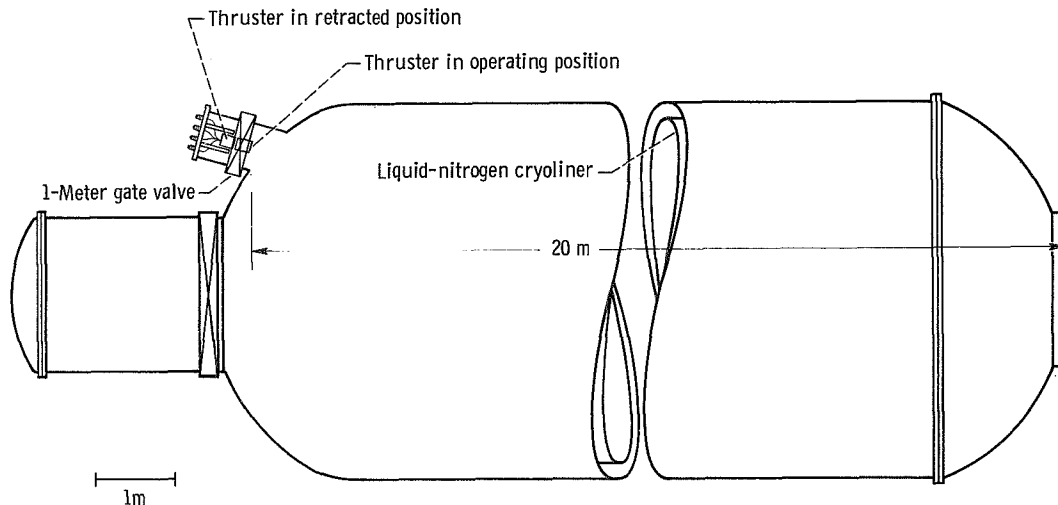


Figure 1. - Thruster mounted in vacuum facility.

A liquid-nitrogen-cooled baffle was used in the main tank to condense the neutral mercury propellant during thruster operation. Pressure in the main tank during thruster operation was normally in the mid- 10^{-7} -torr range, while pressure in the bell jar during operation was usually less than 2×10^{-6} torr.

THRUSTER

The thruster used was a 15-centimeter-diameter, SERT II experimental type, similar to the ones described in references 6 and 7. Figure 2 is a schematic drawing of the thruster. The only major configuration difference was a glass-coated accelerator grid that replaced the double-grid system. Because the cathode baffle configuration has a dominant influence on the discharge chamber voltage (ref. 6), its geometry was modified, as needed, to obtain the desired discharge voltage.

Mercury propellant flow to the thruster manifold was controlled by a 0.63-centimeter-diameter porous tungsten vaporizer (ref. 8). The flow rate to the hollow cathode was controlled by a 0.3-centimeter-diameter vaporizer. The liquid mercury was fed to each vaporizer from precision-bore glass capillaries. By measuring the height change per unit time of the mercury column in the capillary, the average flow rates during the time increment were determined.

The hollow cathode consisted of a 0.32-centimeter-diameter tantalum tube with a thoriated tungsten disk welded to one end. An orifice approximately 0.3 millimeter in diameter was located in the center of the disk. This cathode is heated by means of a swaged wire heated, wrapped, and brazed near the disk (ref. 8). Mercury propellant

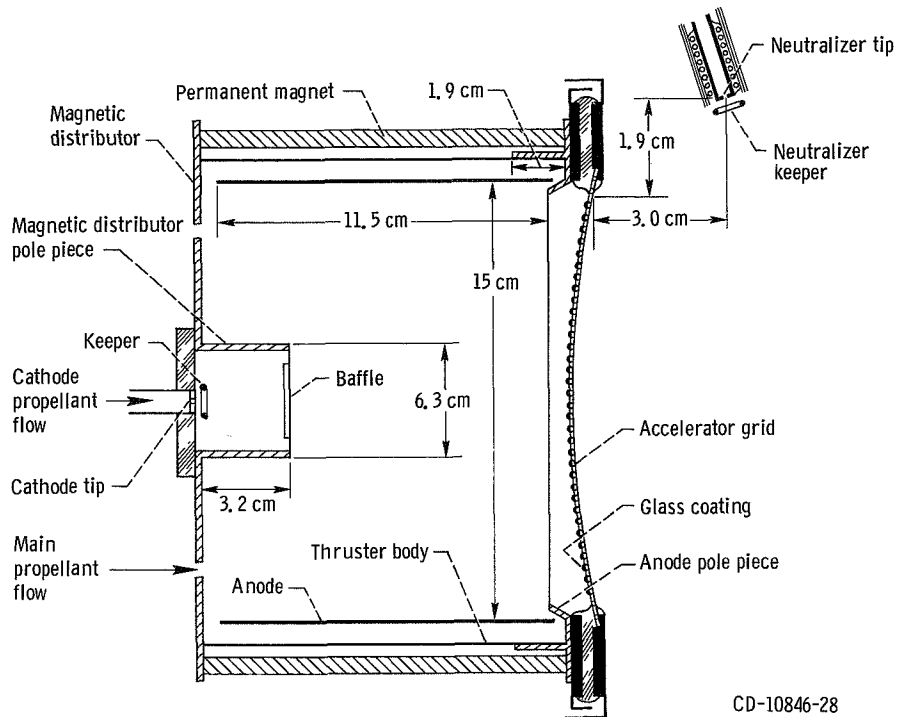


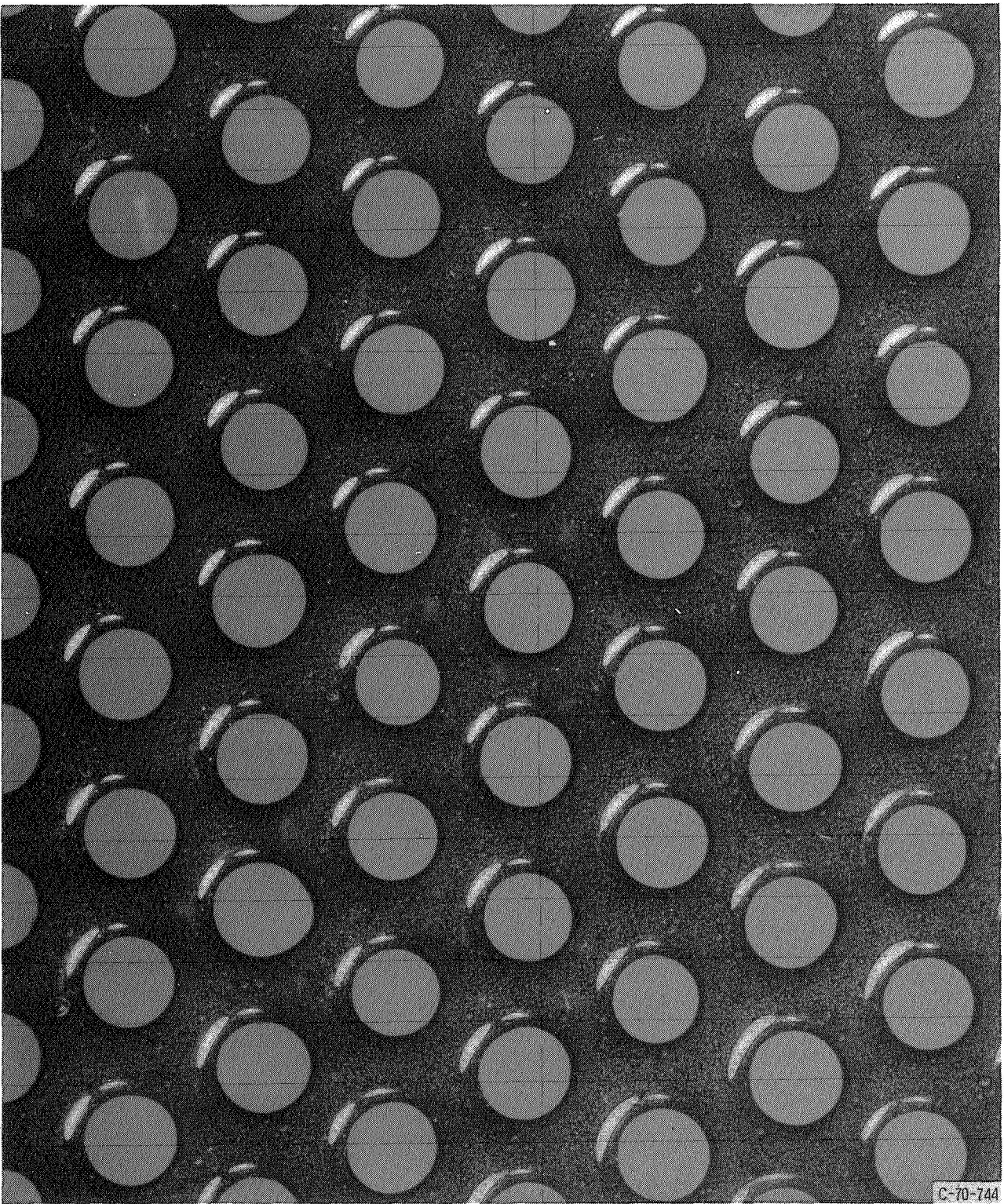
Figure 2. - Section view of 15-centimeter-diameter thruster with glass-coated accelerator grid. (Not to scale.)

was fed through the cathode, and emission current was obtained by placing a 300-volt bias on the cathode keeper electrode (fig. 2). Mercury was then fed into the discharge chamber through the manifold, and the discharge was started by biasing the anode to about 50 volts. The ion beam was extracted by raising the net accelerating electrode potential to approximately 1000 volts positive and biasing the accelerator to approximately 500 volts negative.

ACCELERATOR GRID

Initial Geometry

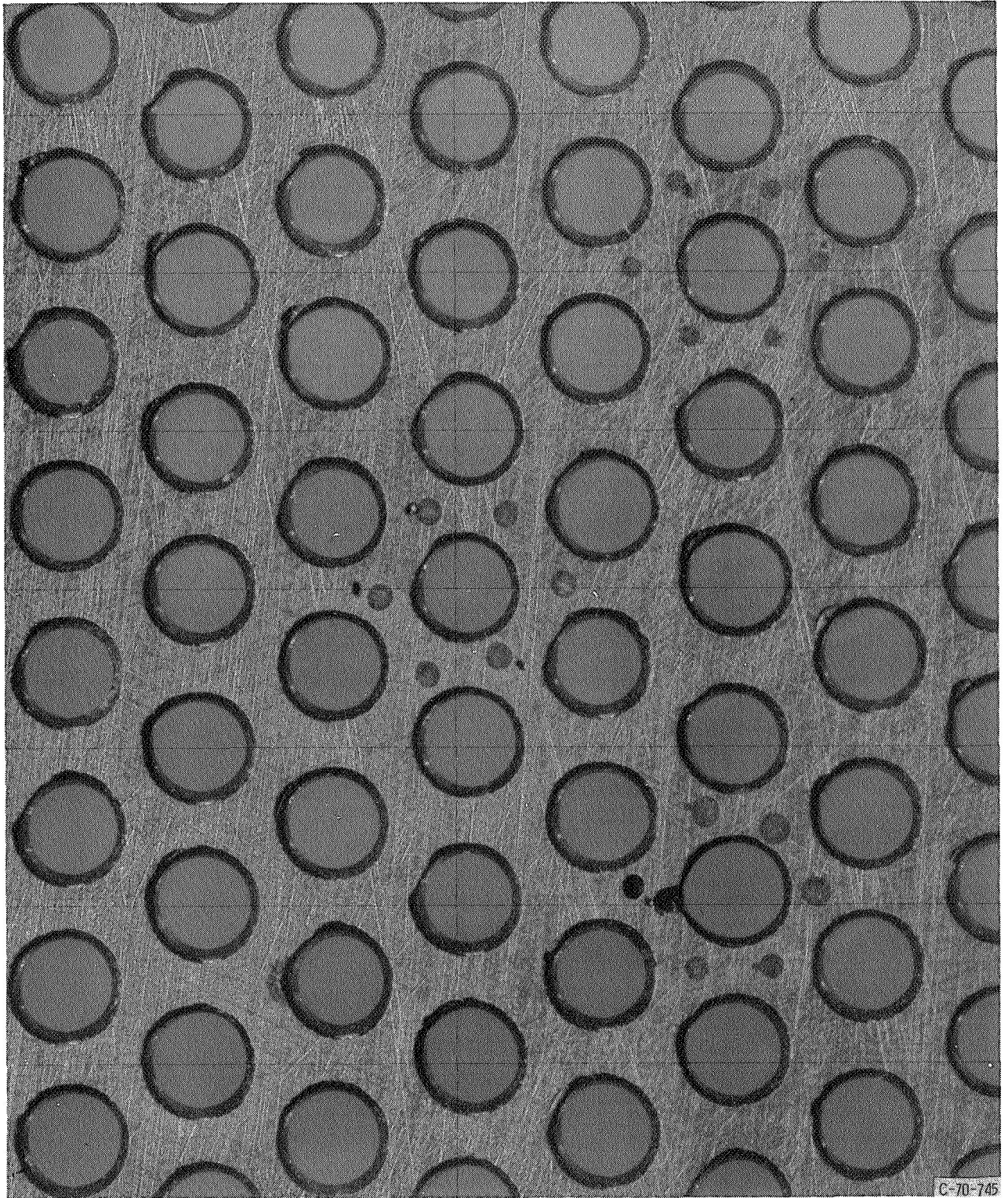
The glass-coated grid for the 15-centimeter-diameter thruster was fabricated by fusing Corning glass (code 7052) to a perforated molybdenum grid. The fabrication process is described in detail in reference 9. Corning glass (code 7052) was chosen for a grid coating material because of its acceptable bonding and electrical resistance characteristics. The 0.38-millimeter-thick molybdenum grid was perforated with 1.9-millimeter-diameter holes hexagonally spaced to provide 51-percent open area. A



1 cm

(a) Glass-coated upstream side.

Figure 3. - Central area of glass-coated grid prior to operation in a thruster.



1 cm

(b) Uncoated downstream side.
Figure 3. - Concluded.

glass slurry consisting of 325-mesh-fineness powdered glass and water was sprayed on the molybdenum and then fired. In order to obtain the desired coating thickness, five sets of sprayings and firings in an oven at 954°C were required. A helium diffusion technique (refs. 4 and 9) was used to minimize the occurrence of bubbles in the glass. The diameter of the perforated region of the glass-coated grid, where all the holes were open and not filled in with glass, was 15.3 centimeters. Beyond this diameter, the holes were filled in with glass because of the grid mounting and retaining ring arrangement. The grid was dished (concave downstream) to a 41-centimeter radius of curvature. The resonant frequency of the most predominant drum mode of oscillation of the grid was 1700 hertz.

The maximum thickness of the glass coating was 0.525 millimeter. This corresponds to 60 percent of the coating stability limit predicted by surface tension forces (ref. 9). The coating stability limit is the maximum thickness of glass which can be applied and still have a glass surface geometry which is stable when the glass is molten during firing. The glass surface tension forces tend to cause the grid holes to fill in with glass during firing if the coating thickness exceeds the stability limit. Because the glass also coats the hole walls, the grid open area is reduced after glass coating. The final physical open area was 33.1 percent with an average hole diameter of 1.54 millimeters. The coated and uncoated sides of the central area of the grid are shown in figures 3(a) and (b), respectively. Also shown in figure 3(b) are several small holes that were drilled through the molybdenum at the location at which charge-exchange erosion pits usually form. The glass filled in these holes during firing. The purpose of this modification was to determine the effect of the glass-filled holes on the charge-exchange erosion pattern and rate. Figure 4 is a view of the entire grid.

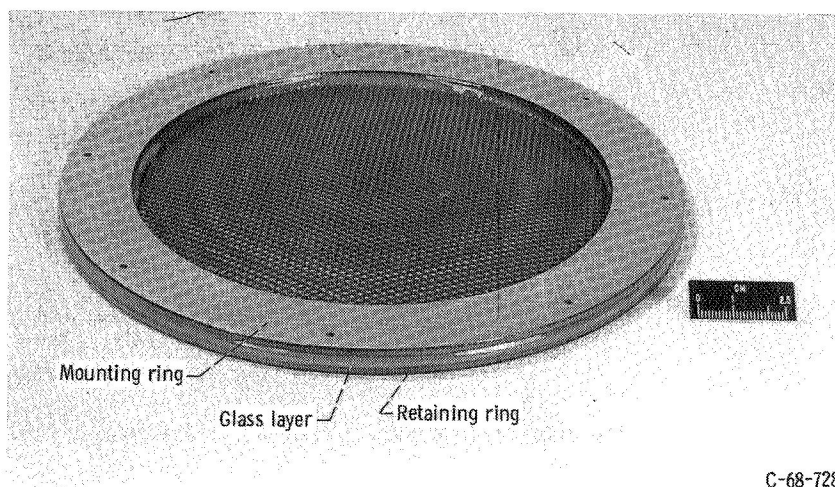
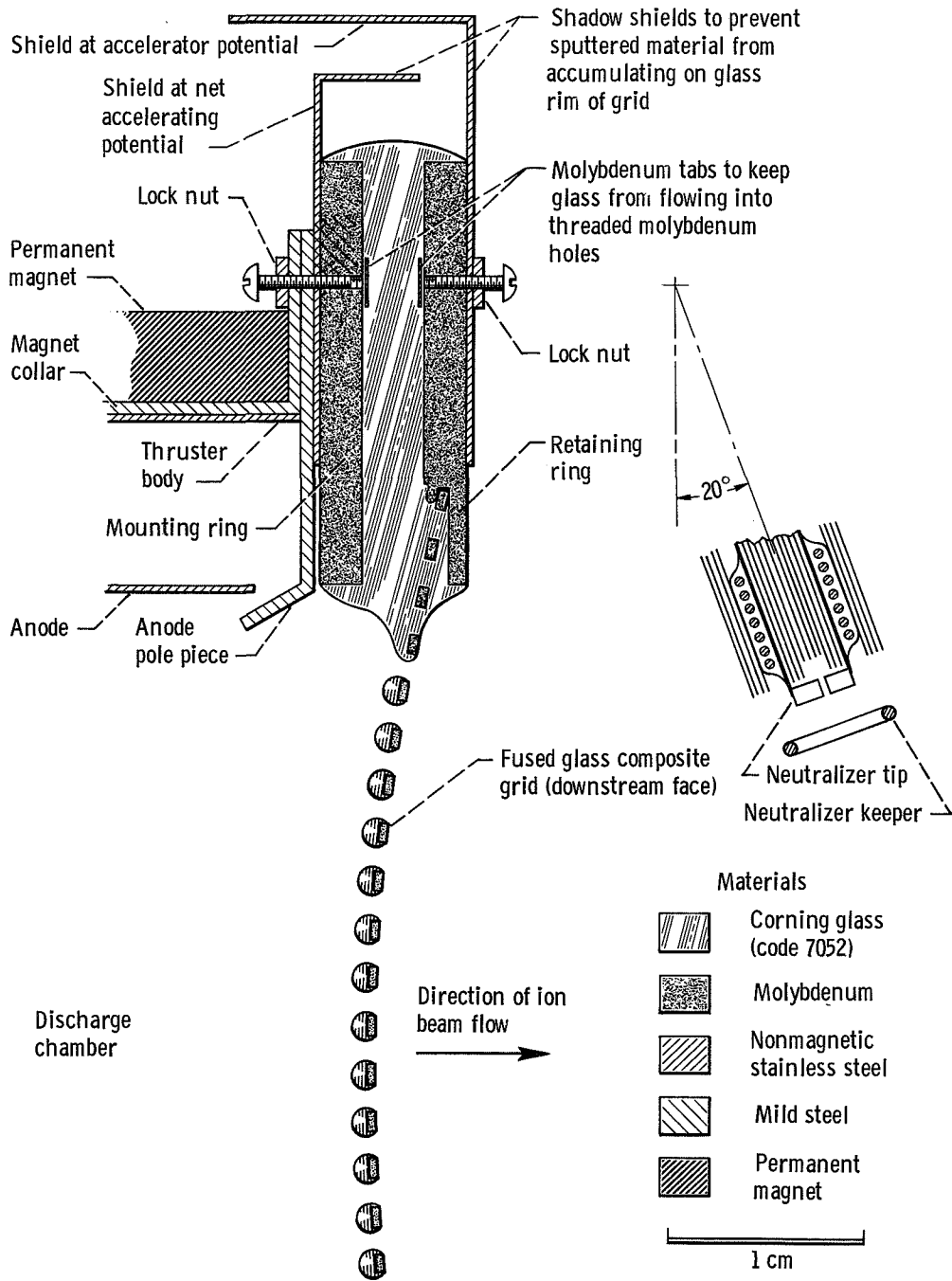


Figure 4. - Perspective view of grid showing mounting ring, retaining ring, and isolating glass layer.

C-68-728



CD-10848-28

Figure 5. - Section view of glass-coated grid, shadow shields, and neutralizer as mounted for operation on thruster for first 508 hours.

Mounting System

The grid was mounted to the thruster using eight 4-40 machine screws which passed through holes in the engine collar and magnetic pole piece and then into holes drilled and tapped in a molybdenum mounting ring (see fig. 5). This mounting ring was electrically isolated from the grid retaining ring by means of a heavy layer of glass approximately 2.54 millimeters thick. The mounting ring was fused to the grid retaining ring during the final grid firing. The shadow shield rings shown in figure 5 were designed to prevent sputtered material from electrically shorting the accelerator-grid retaining ring (at V_A potential) to the mounting ring (near V_I potential).

NEUTRALIZER

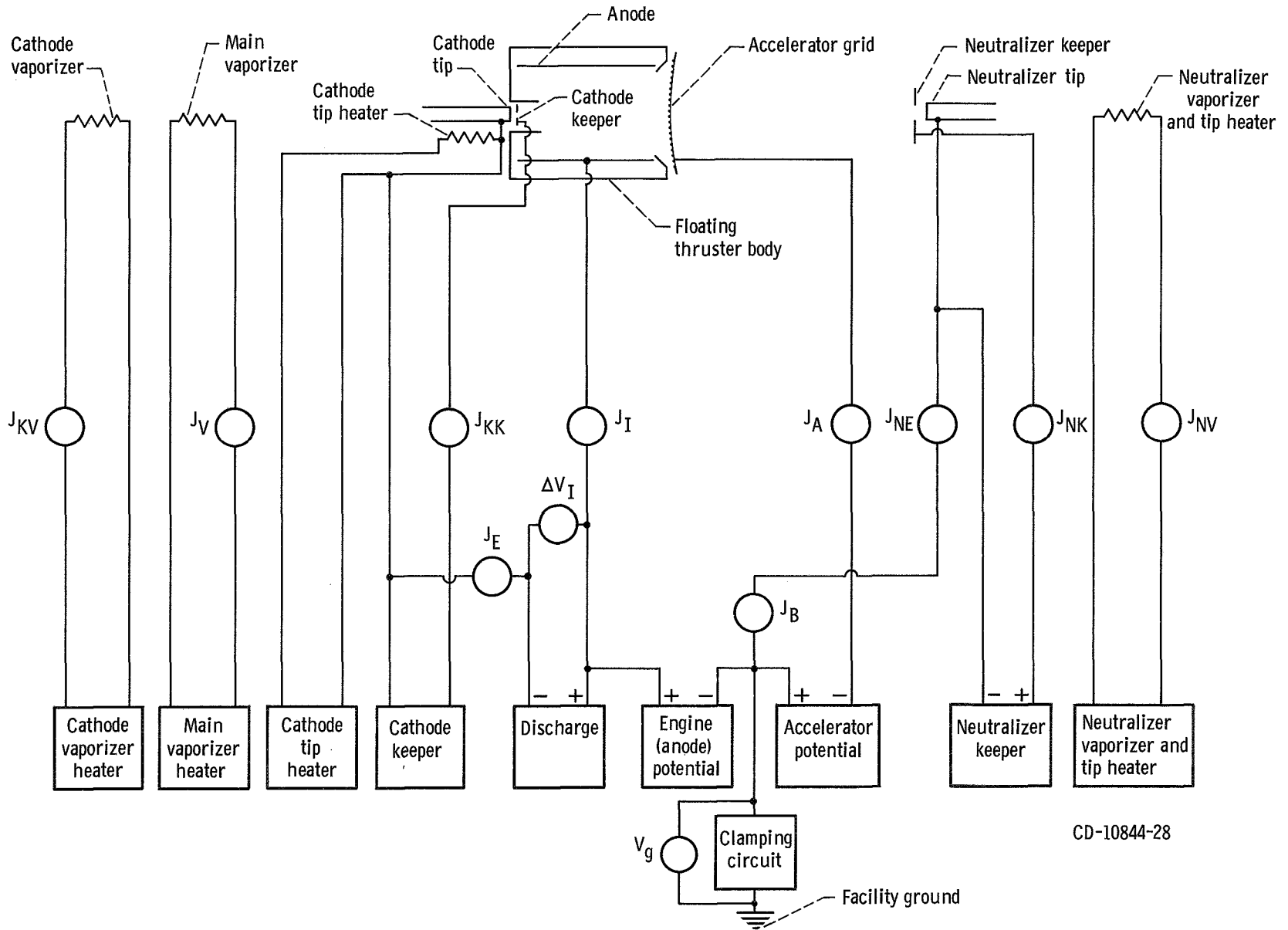
Geometry

The neutralizer used was a plasma bridge, SERT II experimental type (refs. 8 and 10). The neutralizer cathode is identical to the cathode in the discharge chamber. The neutralizer tip (shown in fig. 5) was mounted 3 centimeters downstream of, and 1.9 centimeters radially outward from, the outermost accelerator-grid hole. The neutralizer angle with respect to the accelerator-grid plane was 20° downstream. Both the neutralizer angle and radial location with respect to the outermost grid hole were identical to the SERT II configuration. The SERT II neutralizer axial location is 1.75 centimeters downstream of the flat accelerator grid.

Operation

Neutralizer operation was initiated by introducing mercury vapor through the heated tip and applying approximately 200 volts bias to the neutralizer keeper electrode.

The neutralizer system was electrically floated with respect to tank ground (fig. 6). Because a return ground path is not available for ion beam neutralization, all neutralizing electrons must come from the neutralizer. The neutralizer common point floats at the potential (V_g , with respect to ground) necessary to produce a neutralizer current equal to the ion beam current. The resistance between this common point and the facility ground is greater than 10 megohms, providing a $|V_g|$ of less than 100 volts. The total potential difference (coupling voltage) experienced by the neutralizer electrons is the difference between the beam plasma potential and the neutralizer floating potential. The latter can be measured directly, but the measurement of the former requires prob-



CD-10844-28

Figure 6. - Wiring schematic for thruster.

ing the beam. These voltages are primarily dependent on the neutralizer position and mercury flow rate. Previous tests (ref. 11) have indicated the total coupling voltage is between two and four times the neutralizer floating potential. For safety purposes, a clamping circuit was used to limit the neutralizer floating potential to 100 volts with respect to ground, as shown in figure 6. With the neutralizer emitting electrons to the neutralizer keeper, the current required for neutralization is drawn as soon as the ion beam is extracted, provided the system is floating.

Neutralizer mercury flow was controlled by a 0.3-centimeter-diameter vaporizer identical to the one used for the cathode propellant flow. Mercury was fed to the neutralizer vaporizer from a pressurized reservoir mounted inside the vacuum chamber. Thus, direct flow readings were not made. However, estimates of the flow rate based on the temperature of the vaporizer and temperature-flow calibrations of similar vaporizers are possible.

CONTROL LOGIC

The means of controlling the various thruster parameters are similar to those described in reference 3. Each of the three vaporizers required a servoloop to maintain the required mercury flow rates. In addition, the regulation of either the voltage or current was required in order to fix the steady-state operating point. These control loops are shown schematically in figure 7. The feedback signal and controlled parameter for each control loop are listed in table I and discussed in the following paragraphs.

When the discharge voltage feedback signal is greater than the reference signal, the power to the cathode vaporizer heater and, hence, the cathode propellant flow is increased. Thus, control loop I is an inverting loop. However, control loop II is noninverting. If the beam current feedback signal exceeds the reference signal, the power to the main vaporizer heater; and hence, the main propellant flow, is decreased.

Control loop III is actually a constant current regulator. It is connected in series with the discharge supply and senses the anode discharge current. The feedback signal is then compared to the reference signal. The resulting error signal is used to vary the effective resistance of the series circuit to maintain the preset current.

The response times of the three proportional controllers were varied to eliminate resonant conditions. The solid-state discharge current controller (III) had a response time several orders of magnitude less than any other controller response time. The discharge voltage control loop (II) had a response time of the order of seconds (excluding thermal response of the cathode vaporizer). The beam current control loop (I) had a response time of the order of tens of seconds. Thus, control loop I would respond only to definite extended-time off-normal beam current conditions. Control loop II would respond to any off-normal discharge voltage condition except fast transients. In

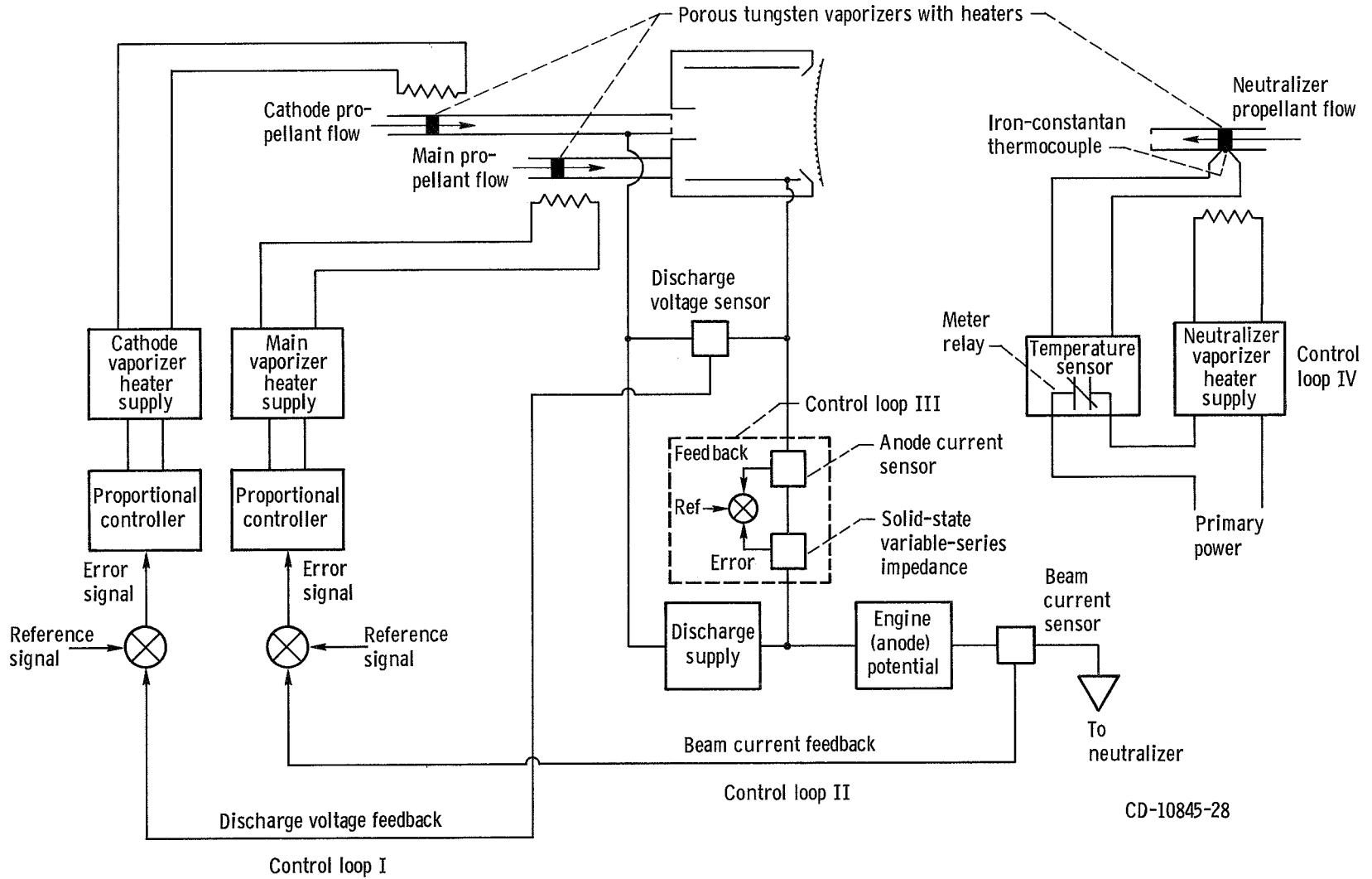


Figure 7. - Control system for thruster.

TABLE I. - SUMMARY OF CONTROL LOOP PARAMETERS

Control loop	Type	Sensed (feedback) parameter	Controlled parameter	Reaction
I $\Delta V_I - J_{KV}$	Proportional	Discharge voltage	Cathode vaporizer power (cathode propellant flow)	Increase in vaporizer power causes decrease in voltage (inverting)
II $J_B - J_V$	Proportional	Beam current	Main vaporizer power (main propellant flow)	Increase in vaporizer power causes increase in beam current (noninverting)
III $J_I - J_I$	Proportional	Discharge current	Discharge current	Constant current regulator
IV $T_{NV} - J_{NV}$	On-off	Neutralizer	Neutralizer vaporizer power (neutralizer propellant flow)	Increase in temperature above set point causes vaporizer power to be turned off until temperature is sufficiently reduced

addition, control loop II changes essentially occurred at a constant main propellant flow because of the difference in time constants. Control loop III would respond to all off-normal discharge current conditions, including transients.

Although it is possible to control the neutralizer mercury flow with a proportional controller by using the neutralizer anode voltage as a feedback signal (ref. 8), a simpler on-off controller was used for these tests. A thermocouple was used to monitor the neutralizer vaporizer temperature. The output was fed to a meter relay. When the thermocouple output indicated a temperature in excess of the set-point temperature, the vaporizer heater power was turned off. When the temperature fell below the set point, the power was restored.

Although such a system is adequate for experimental purposes, it is not suited for a refined control system because there is no guarantee that the propellant flow will remain unchanged for a given vaporizer temperature for extended periods. For a refined system, a proportional controller which does not depend on temperature is far superior.

One problem experienced with control loop II was the effect of the high voltage (engine potential and accelerator potential) on the discharge chamber voltage. When high voltage was removed, as in the case of a breakdown, the discharge chamber voltage decreased. This caused the controller to reduce the cathode vaporizer heater power in an attempt to raise the discharge voltage. If the time required to raise the high voltage is long enough, the heater power would be reduced to the point where the cathode propellant flow was too small to maintain cathode emission, and the discharge would be ex-

tinguished. This problem was eliminated by using an auxiliary power supply to maintain a minimum vaporizer heater power. This heater power was chosen to correspond to a cathode propellant flow sufficient to maintain cathode emission for periods of hours. Because the other proportional controllers were noninverting, they did not have similar problems.

UNATTENDED THRUSTER OPERATION

Both the vacuum facility and the thruster were capable of running unattended for periods of days. Critical operating parameters were sensed and any off-normal conditions in excess of the preset limitations caused shutdown of the facility, the thruster, or both. Facility shutdown conditions are detailed in reference 12.

Those conditions which were considered sufficient for a thruster shutdown are listed in table II. Figure 6 shows that the beam current and neutralizer emission current are

TABLE II. - OFF-NORMAL EVENTS WHICH
CAUSE THRUSTER SHUTDOWN

Event	Duration, sec	Reason for shutdown
Low neutralizer or beam current ($J_{NE} = J_B$)	30	Lack of proper neutralization could cause grid damage
High neutralizer or beam current ($J_{NE} = J_B$)	30	High neutralizer emission could cause grid damage
High accelerator drain current, J_A	30	Damage to grid could occur or may already have occurred
High discharge current, J_I	30	Possible damage to cathode

equal for a neutralizer floating configuration. In the event of the clamping circuit grounding the neutralizer, the current through the meter relay would be near zero. Thus, if the clamping circuit operated for any reason, a thruster shutdown resulted.

A low beam current and/or neutralizer current indicated either a thruster failure or a neutralizer failure resulting in the grounding of the system through the clamping

circuit. A high beam current and/or neutralizer current indicated either a faulty control system which could not reduce the beam current or electron backstreaming which appeared as an erroneously high beam current reading. High accelerator-grid drain current J_A indicated a possible grid failure or some condition which might lead to a grid failure. The discharge current J_I was monitored to prevent damage to the cathode caused by high emission current in the event of a failure of the discharge current regulator (control loop III).

Each high-voltage power supply was reset after a breakdown by a meter relay system which raised or lowered the primary power as long as the voltages were below or above the set points. Because a direct short from thruster potential to the accelerator or to ground would cause continuous recycling of the power supplies, a counter and a timer system were included. The system was programmed to count the number of breakdowns which occurred within a preset time interval. A shutdown would result if the counter exceeded a preset number of breakdowns within the time interval.

Periodic recordings of critical electrical parameters were made during unattended operation. No mercury flow measurements were made during these periods.

RESULTS AND DISCUSSION

The performance of the thruster is shown in figure 8. Data were recorded hourly except for periods of unattended thruster operation. The average value of a parameter during each interval of the run was determined by measuring the area under the curves and dividing that area by the number of hours in the interval. These average values are shown in columns 1 to 7 of table III, which is a summary of the grid and thruster geometry and operating conditions. For purposes of discussion, the 1000-hour test has been divided into eight intervals based on times when changes in cathode baffle geometry or grid edge termination were made.

The average cathode and main propellant flows were determined by averaging the individual, hourly propellant flow readings. In some cases, air trapped in the flow-measuring capillary tubes or slight leaks in the feed system made accurate flow measurements impossible. The various propellant flows and average propellant utilization efficiencies are given in columns 8 to 11. Column 12 lists the discharge chamber losses based on the average performance listed in columns 1 to 8.

The typical operating ranges of the neutralizer parameters are presented in columns 13 to 15. Although the neutralizer was not a prime consideration in this test, the lack of significant grid erosion in the vicinity of the neutralizer is of interest. The neutralizer keeper voltage and voltage to ground are in the same range as in the majority of tests previously reported with conventional double-grid systems and in which

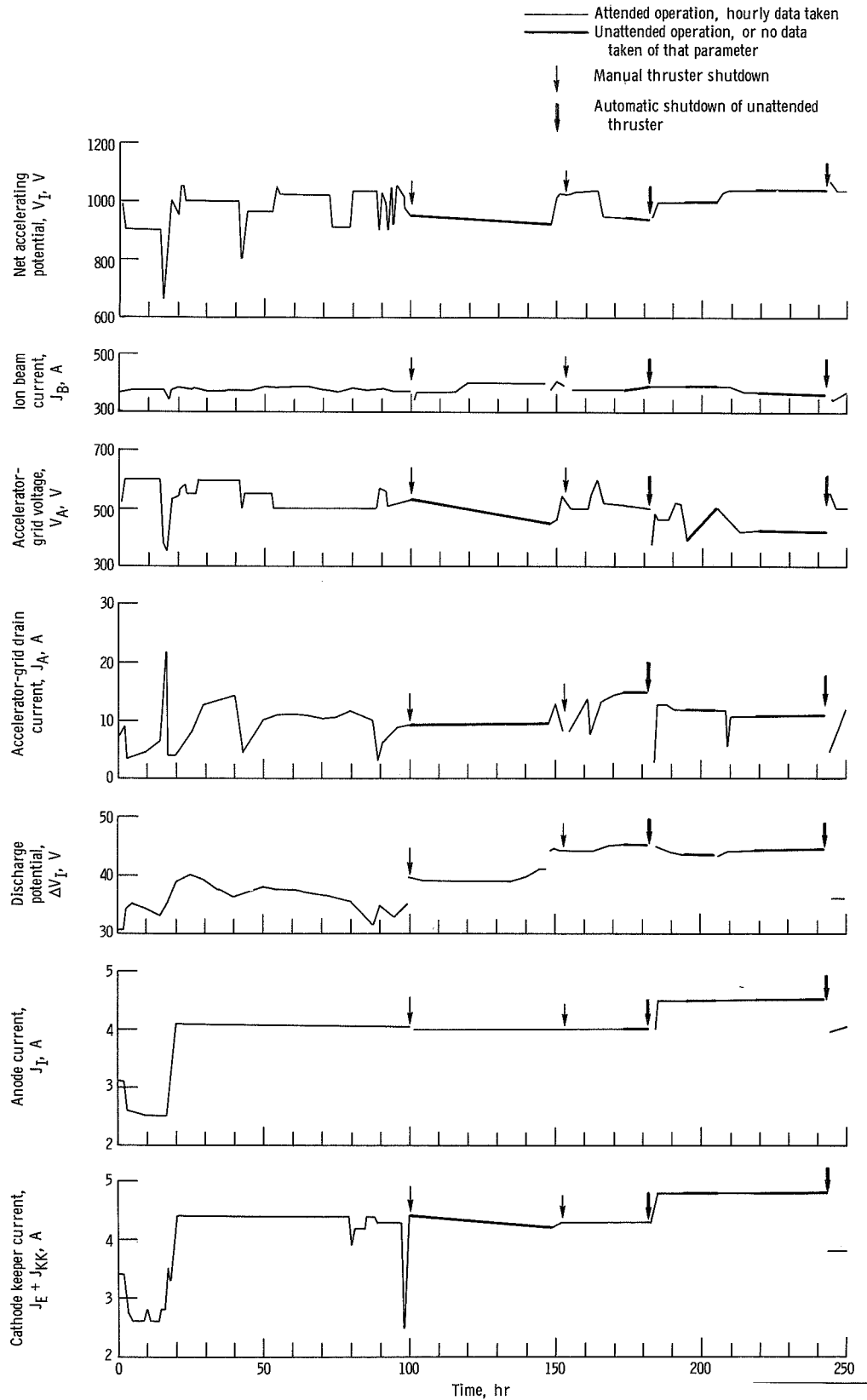


Figure 8. - Hourly performance plot of thruster parameters.

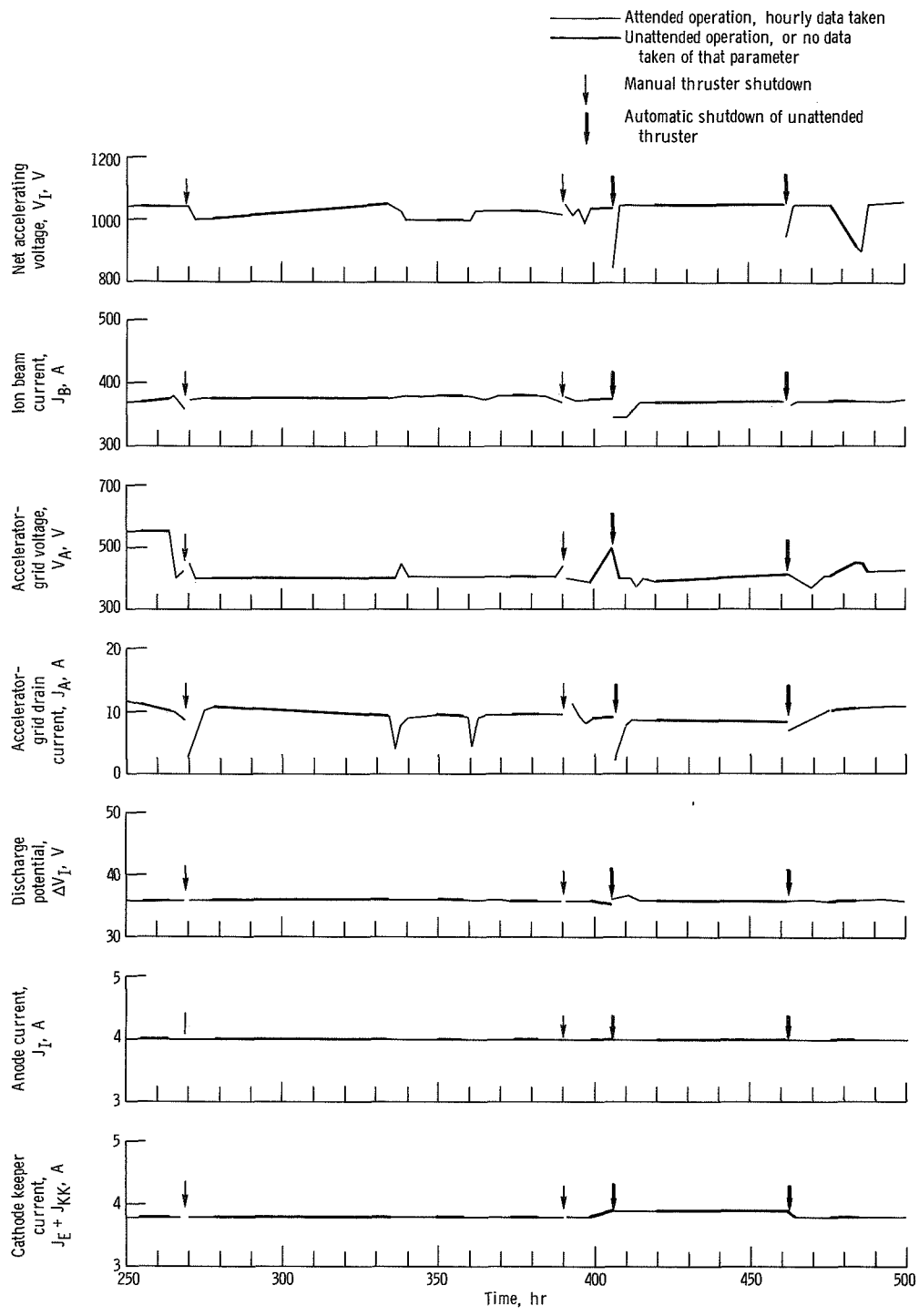


Figure 8. - Continued.

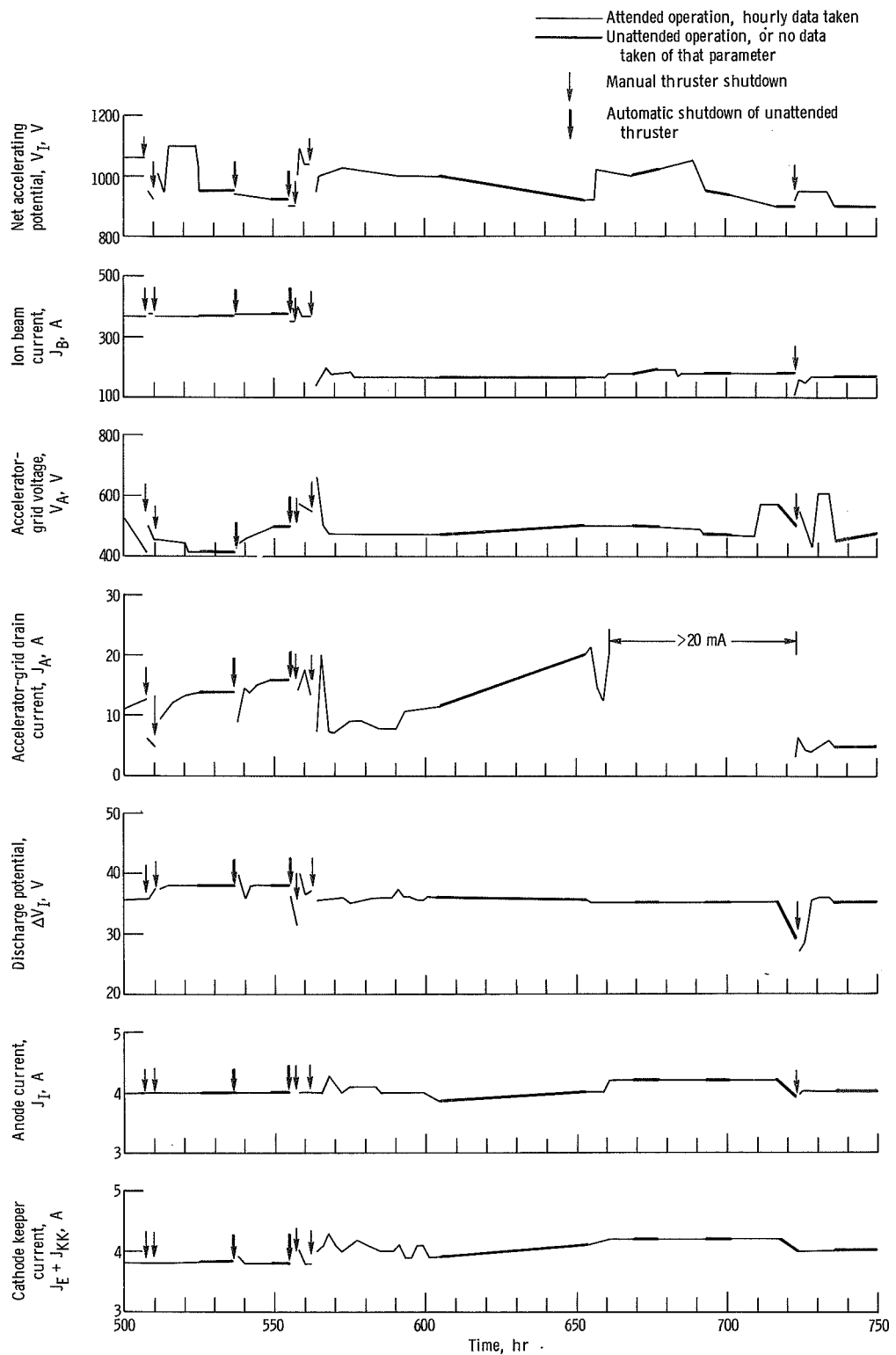


Figure 8. - Continued.

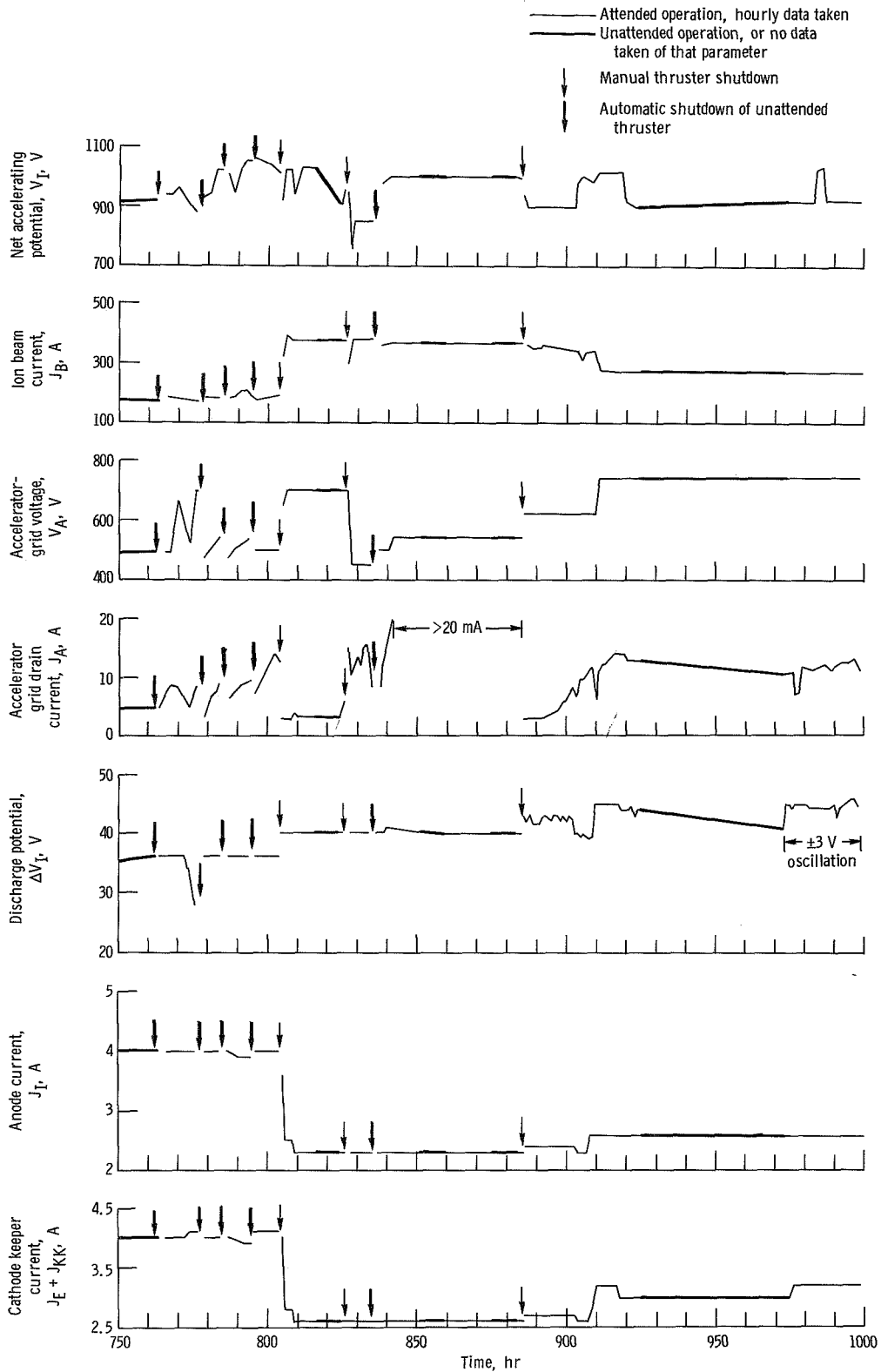


Figure 8. - Concluded.

TABLE III. - SUMMARY OF THRUSTER GEOMETRY AND OPERATING CONDITIONS

Run hours	1	2	3	4	5	6	7	8	9	10
	Engine (anode) potential, V	Beam current, mA	Accelerator potential, V	Drain current, mA	Discharge voltage, V	Anode (discharge) current, A	Total emission current, A	Cathode propellant flow, mA	Main propellant flow, mA	Total propellant flow, mA
0 to 100	990	373	456	9.4	37.6	4.00	4.06	23	----	----
100 to 243	990	373	456	9.4	37.6	4.00	4.06	^b 74	^b 309	^b 383
243 to 508	990	373	456	9.4	37.6	4.00	4.06	47	338	385
508 to 557	969	363	432	12.5	37.2	3.97	3.80	67	336	403
557 to 564	1021	376	576	12.9	36.5	3.92	3.70	--	313	---
564 to 804	971	176	482	13.7	34.8	4.02	4.02	28	159	187
804 to 885	978	375	558	16.6	39.8	2.32	2.65	49	339	388
885 to 1000	924	301	705	10.4	43.0	2.49	2.93	52	269	321

Run hours	11	12	13	14	15	16	17	18
	Propellant utilization efficiency, percent	Discharge losses, eV/ion	Neutralizer anode voltage, V	Neutralizer ground voltage, V	Neutralizer vaporizer temperature, °C	Cathode number	Grid configuration ^a	Baffle configuration
0 to 100	----	366	20 to 23	15 to 20	320	1	A	Six-hole SERT II type
100 to 243	97.4	366	^b 25 to 30	^b 30 to 37	^b 329	1	↓	2.54-cm solid
243 to 508	96.9	366	14 to 43	20 to 43	328	2	↓	2.06-cm solid
508 to 557	90.2	370	18 to 32	19 to 25	328	(c)	↓	2.06-cm solid
557 to 564	----	344	13 to 28	-----	316	↓	B	(d)
564 to 804	94.2	760	10 to 40	13 to 21	304 to 327	↓	C	↓
804 to 885	96.7	206	9 to 15	-----	324 to 371	↓	D	↓
885 to 1000	94.3	313	9 to 10	-----	337 to 360	↓	E	↓

^aGrid configuration: A - unterminated original grid; B - 13.2-cm-diameter insulating mask; C - 8.9-cm-diam insulating mask; D - metal mask (single); E - metal mask (double) with sputter shield.

^bExcludes run hours 100 to 148.

^cNot documented.

^dVarious solid baffle diameters.

grid erosion was experienced (refs. 8 and 11). Although the neutralizer flow was not measured nor the vaporizer calibrated, other vaporizers similarly made from the same porous tungsten stock typically operate between 10 and 80 equivalent milliamperes of neutral mercury flow for the temperatures shown in column 15. The final three columns show the various configuration modifications.

FIRST 508 HOURS OF TEST

During the first 100 hours, the thruster was operated at a very low cathode flow with a discharge chamber voltage of 35 to 40 volts. At the end of the first 100 hours, a baffle change was made to permit operation at the same discharge voltage with a higher cathode propellant flow rate (ref. 6). The increased cathode flow provided more stable thruster operation. After run hour 243, the cathode, having been operated at 4 amperes emission current (approximately twice SERT II levels) was removed for inspection. The results of this inspection indicated that the cathode wear rate was greater at higher emission currents. This result was reported in reference 11. During this segment of the test, electron backstreaming was observed when the accelerator-grid potential was set more positive than -375 volts at the same time that $J_B = 375$ milliamperes and $V_I = 1000$ volts. The thruster was restarted with a new cathode at an emission current of about 4 amperes.

At the end of run hour 508, the grid was removed for a detailed inspection.

Accelerator-Grid Drain Current

The accelerator-grid drain current is a meaningful indication of grid degradation. This current may be caused by one or all of the following four mechanisms:

- (1) Primary ion impingement
- (2) Surface conductivity of sputtered material shorting the accelerator-grid retaining ring (at V_A potential) to the mounting ring (near V_I potential)
- (3) Electrical volume conductivity of the glass coating
- (4) Charge-exchange ion impingement

Primary ion impingement. - It is believed unlikely that primary ions extracted from the discharge chamber plasma sheath slightly upstream of the glass coating would strike the downstream face of the accelerator grid. Primary ion impingement on glass-covered surfaces was thought to be small. These surfaces included the hole walls and upstream surface of the accelerator grid. Primary ion impingement could occur, however, in places where the glass coating had been removed because of an electrical breakdown.

After 508 hours of operation, there were numerous electrical breakdown sites near the peripheral holes in the accelerator grid. The most extensive breakdown site of this type is shown in figure 9. This damage was thought to be caused by the deposition of a layer of conductive sputtered material on the glass coating near the outermost holes in the grid. The accumulation of a conductive sputtered coating could eventually lead to electrical breakdown or high drain current from the discharge plasma, across the

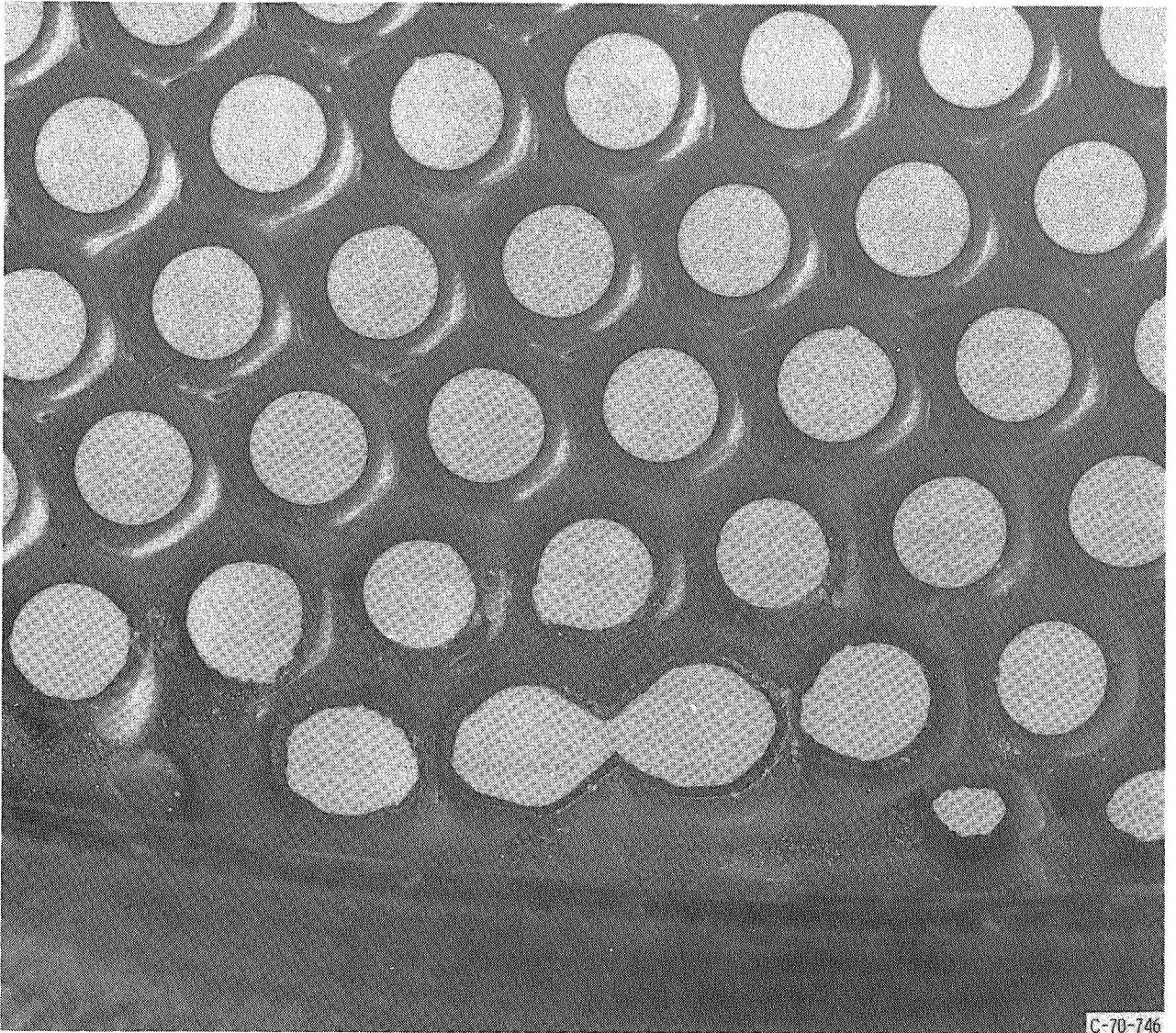


Figure 9. - Largest breakdown site in grid after 508 hours of operation.

sputtered coating on the glass hole walls, to the accelerator grid. This problem occurred near the periphery of the grid, the region where the ion current density is known to be low. This, in turn, suggested that ion sputter cleaning of the glass may be occurring in the central region of the grid.

A method to maintain a sputter cleaning rate in excess of the deposition rate of material on the glass coating near the grid edge appeared desirable. A proposed approach was to reduce the grid active diameter and maintain the same ion beam current. In this way, the outermost holes would have a higher ion current density for sputter cleaning. To verify this hypothesis, a second grid was fabricated and operated for 115 hours.

The 115-hour test grid had a 13-centimeter-diameter active area. This grid, shown in figure 10, had all holes beyond a 13-centimeter diameter filled in with glass. This

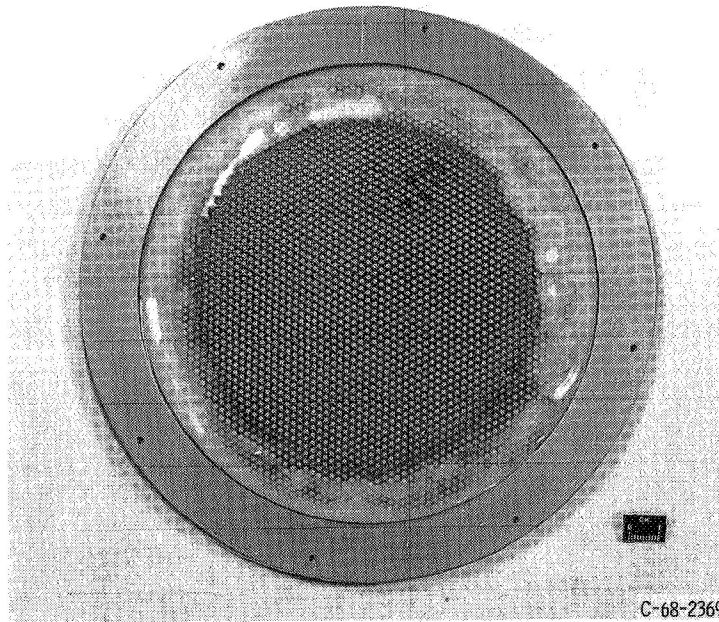


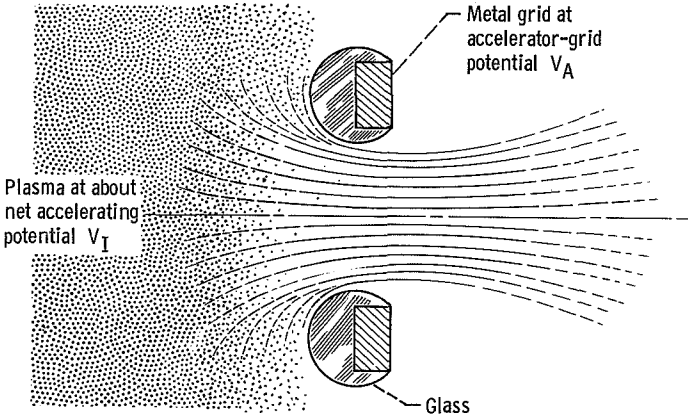
Figure 10. - Thirteen-centimeter-diameter-active-area glass-coated grid.

test is not included in table III. The test indicated that edge breakdown was resulting from a thinner-than-average glass coating near the edge of the grid. Glass surface tension forces during fusing of the glass to the grid caused the glass to be thinner where there was a transition from a glass-coated area with holes to an area without holes. Thus, all the metal webs at the outer edge of the grid active area were coated with less glass than those in the central area of the grid. The result of this test led to the conclusion that the general grid degradation observed after the 508-hour test interval was caused by thin glass at the grid edges rather than the lack of sputter cleaning. Of course, once the breakdowns have occurred, direct ion impingement that will continue to remove the glass and metal is likely. An exception arises when the breakdown site is small and located along a line of symmetry of the hexagonal hole array (see appendix B). As discussed in appendix B, for this special case, experiments have shown that breakdown sites only cause short-term high accelerator drain current, and the rate of sputter damage drops off after the sputtering has completely eroded a hole through the accelerator-grid metal. After that, the breakdown site acts like a small accelerator-grid hole, and only slow degradation, if any, can be detected on the grid.

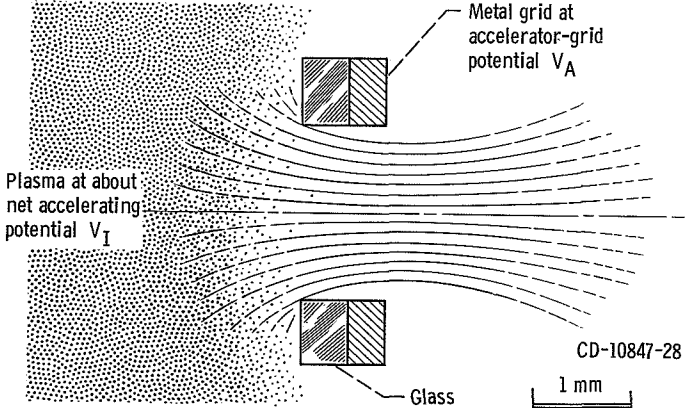
If the glass coating is thin, the most probable place for breakdown is not near the line of symmetry but near the upstream corners of the hole wall. Breakdown in these areas is a catastrophic process which continues to cause an enlarging of the breakdown site and produces high accelerator drain currents as a result of direct impingement. This process is thought to be the cause of the damaged region shown in figure 9.

Surface conductivity of sputtered material. - At the time of the 508-hour inspection, there was no sign of arcing between the accelerator-grid retaining ring and the mounting ring caused by the surface conductivity of the sputtered material on the glass. There was, however, visible evidence of a deposit of sputtered material being built up on the glass surface between the molybdenum rings. The shadow shields on the outermost radial portions of the accelerator-grid retaining and mounting rings adequately prevented any noticeable sputtered material from depositing on the outer glass edge (see fig. 5).

Electrical volume conductivity of glass coating. - The electrical volume conductivity of the glass coating during thruster operation may contribute to the observed accelerator-grid drain current if the grid temperature is high enough. Figure 11(a)



(a) Typical glass-coated-grid geometry.



(b) Model cross section used for conductivity calculation.

Figure 11. - Composite grid cross section of a single hole.

shows a sketch of the cross section of the glass-coated grid. Figure 11(b) shows the geometry used to calculate values for the magnitude of the accelerator drain current that might arise because of the electrical volume conductivity of the glass. If the electrons flow from the metal accelerator grid through the glass to the surface of the glass exposed to the discharge plasma (as in fig. 11(b)), the accelerator drain current J_A due to this glass conductivity is

$$J_A = \frac{\pi(V_I - V_A)(1 - F_m)d^2}{4\rho L_g} \quad (1)$$

where V_I is the net accelerating potential, V_A is the accelerator-grid potential ($V_A < 0$), F_m is the grid fraction of metallic open area, d is the grid diameter, ρ is the resistivity of the glass, and L_g is the thickness of the glass coating. The model used assumes that the temperature is uniform across the grid except at the rim, where the glass is assumed to be cooler, resulting in a negligible drain current between the molybdenum mount rings. The temperature-dependent value for the resistivity ρ of Corning glass (code 7052) is given by

$$\rho = 0.142 \exp \left[\frac{1.956 \times 10^{-19}}{kT_g} \right] \quad (2)$$

where ρ is expressed in ohm-meters, k is the Boltzmann constant and equal to 1.38×10^{-23} joules per K, and T_g is the glass temperature in Kelvin. A plot of accelerator drain current (as expressed in eq. (1), using eq. (2) for the resistivity) for typical values of V_I , V_A , F_m , d , and L_g over a range of temperatures is shown in figure 12. At temperatures above 500°C , the drain current due to glass conductivity rises sharply with increasing temperature and could easily account for the average 9.4 milliamperes of accelerator drain current if the grid temperature was 633°C .

Charge-exchange ion impingement. - The last major source of accelerator drain current is the current caused by the arrival of mercury charge-exchange ions on the downstream face of the accelerator grid. This source of drain current should have amounted to only a small fraction of the total measured drain current because of the high propellant utilization efficiency (over 90 percent). The sputtered erosion pattern near the neutralizer area of the grid was not noticeably different than the charge-exchange erosion pattern over the remainder of the downstream grid surface. In contrast to results reported in references 8 and 11, this indicates that neutrals and ions emitted from the plasma bridge neutralizer were not a significant contribution to the accelerator drain current.

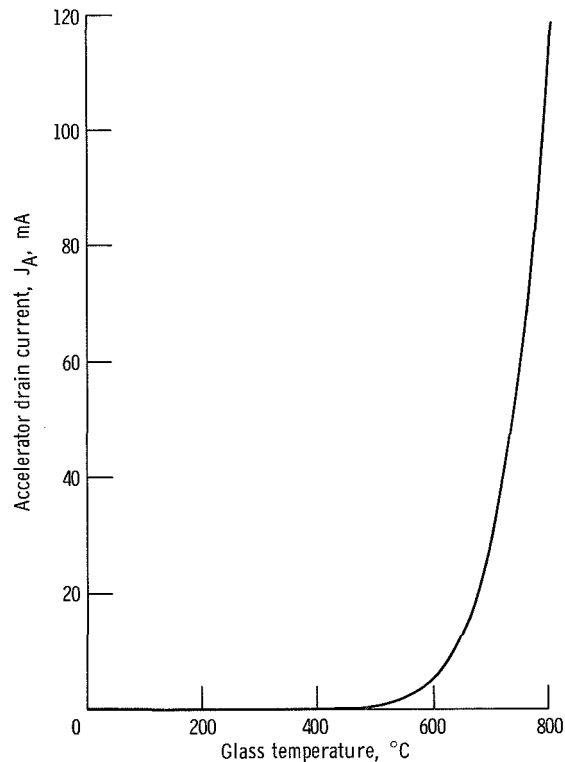
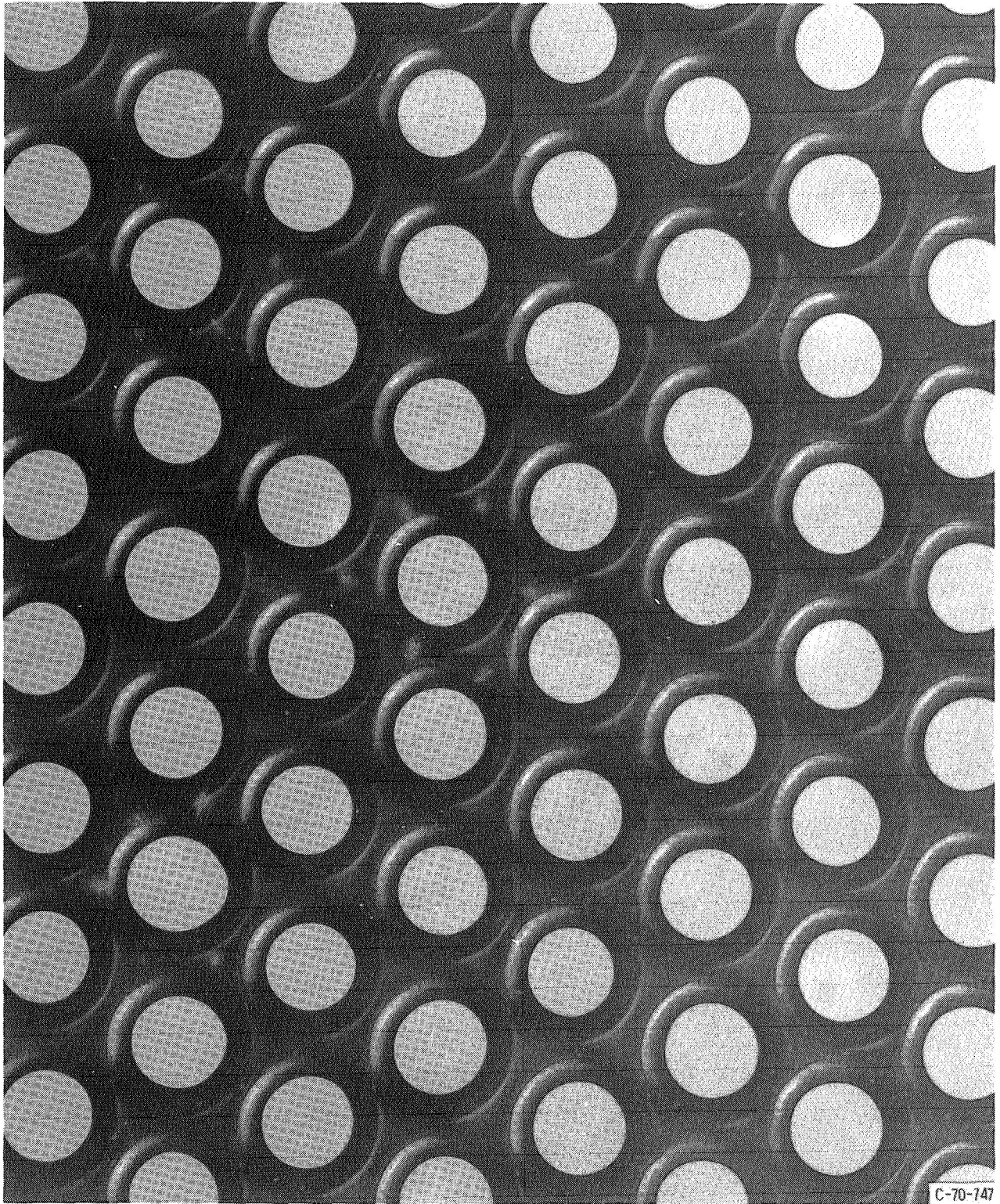


Figure 12. - Theoretical accelerator drain current due to glass volume conductivity as a function of glass temperature. From equations (1) and (2). Net accelerating potential, $V_T = 990$ volts; accelerator-grid potential, $V_A = -450$ volts; grid fraction metallic open area, $F_m = 0.51$; grid diameter, $d = 15$ centimeters; glass coating thickness, $L_g = 0.525$ millimeter.

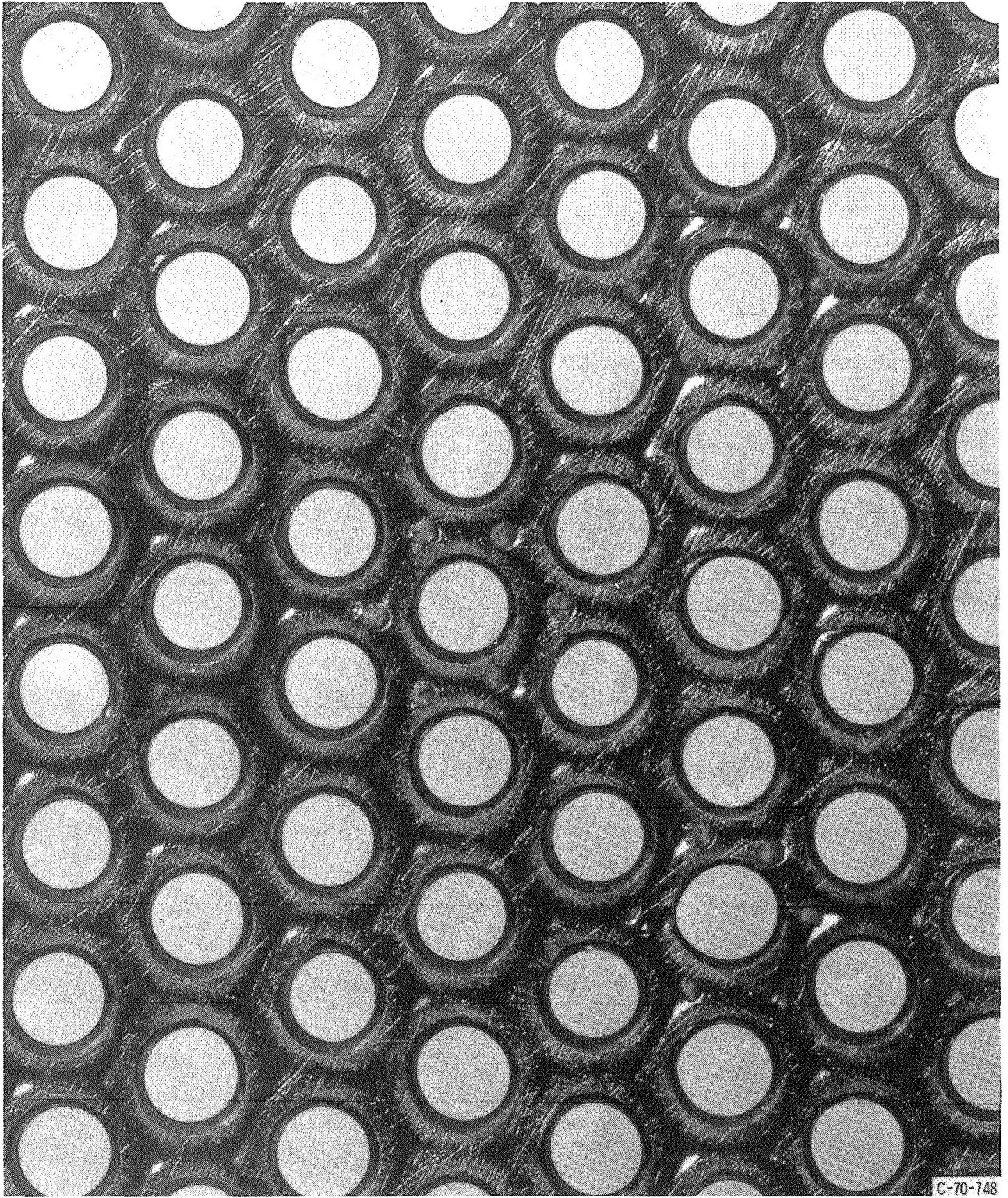
Accelerator-Grid Lifetime Estimates

Figures 13(a) and (b) show the upstream and downstream surfaces, respectively, of the central area of the grid after 508 hours of operation. These figures can be compared with figures 3(a) and (b), which show this same area before the test. Slight erosion can be seen on both the coated and uncoated sides of the grid.

Weight loss. - The initial weight of the grid (including the retainer and mounting ring) was 730.292 grams. After 508 hours of operation, a weight loss of 1.074 grams was measured. From weight measurements made on other grids of similar geometry, it was estimated that the 15.3-centimeter-diameter active ion extraction region of the grid consisted of 35 grams of molybdenum and 12 grams of glass. If the weight loss is assumed to be caused by grid erosion in this region only, the maximum possible grid lifetime would be less than 22 200 hours, at which time all the grid would be consumed. This estimate assumes that the rate of weight loss remains constant. However, a large



(a) Glass-coated upstream face of grid,
Figure 13. - Central area of grid after 508 hours of operation.



(b) Uncoated downstream face of grid.

Figure 13. - Concluded.

portion of the measured weight loss may be caused by the peripheral breakdown sites and subsequent sputter erosion, which implies a much shorter lifetime. If this is a significant fraction of the weight loss, a proper grid-edge-termination geometry would probably extend the projected lifetime. This is because the low weight-loss rate of the central area of the grid would then be the lifetime-determining criterion.

Glass erosion. - Some erosion of the glass from the sides of the holes has occurred. The abrupt change in reflected light (see fig. 13(a)) around each hole is a result of this erosion. The cause of the hole-wall erosion is thought to be the result of sputtering by grazing primary ions. The measured amount of the increase in hole diameter in 508 hours of operation was approximately 0.005 millimeter. Ion impingement on the molybdenum grid itself would occur when the glass lining, measured to be 0.0185-centimeter thick, has been completely removed. (Glass thickness measurements were made from photomicrographs.) At this rate, there is sufficient glass lining the hole walls to permit 37 000 hours of operation. At this time, direct ion impingement would occur around the hole walls. Although this calculation may be in error because of the small value of erosion rate used, it seems to indicate that other failure mechanisms may be more pertinent.

Molybdenum erosion. - The charge-exchange ion erosion pattern in the molybdenum grid shown in figure 13(b) is similar to that occurring with double-grid ion extraction systems. Charge-exchange erosion pits occur at the intersection point of three metal webs and shallower grooves occur along the webs connecting these pits. Measurements were made in the central area of the grid where the most severe charge-exchange ion sputtering erosion had occurred.

The deepest erosion pit was 0.0685-millimeter deep. Assuming a constant rate of pit depth increase, 2720 hours of sputtering would be required for the bottom of the deepest pit to be at the plane of the glass-to-metal seal. This would probably not cause any grid failure because the erosion rate of the glass would be small and the pit width would instead increase. As can be seen in figure 13(b), there are three holes surrounded by glass-filled holes at the web intersections. This modification was intended to display the effect of glass at the charge-exchange erosion site. The erosion in these glass site areas appears to have shifted away from the normal point of symmetry probably because of surface charges built up on the exposed glass. However, the net amount of erosion, although slightly relocated, appeared to be the same as on other areas of the grid.

Measurements of the depth of the grooves in the molybdenum webbing midway between the charge-exchange pits indicated that the deepest groove was in the central area of the grid and was 0.0254 millimeter deep with average values of 0.0076 millimeter. Assuming a constant rate of average depth increase with time in the grooves, a maximum grid lifetime of 25 000 hours is predicted. After this amount of time, the central area of the grid should have several electrically isolated hexagons which would allow electron

backstreaming to take place. All the calculated lifetime predictions are based on the assumption that a proper grid-edge-termination scheme could be provided.

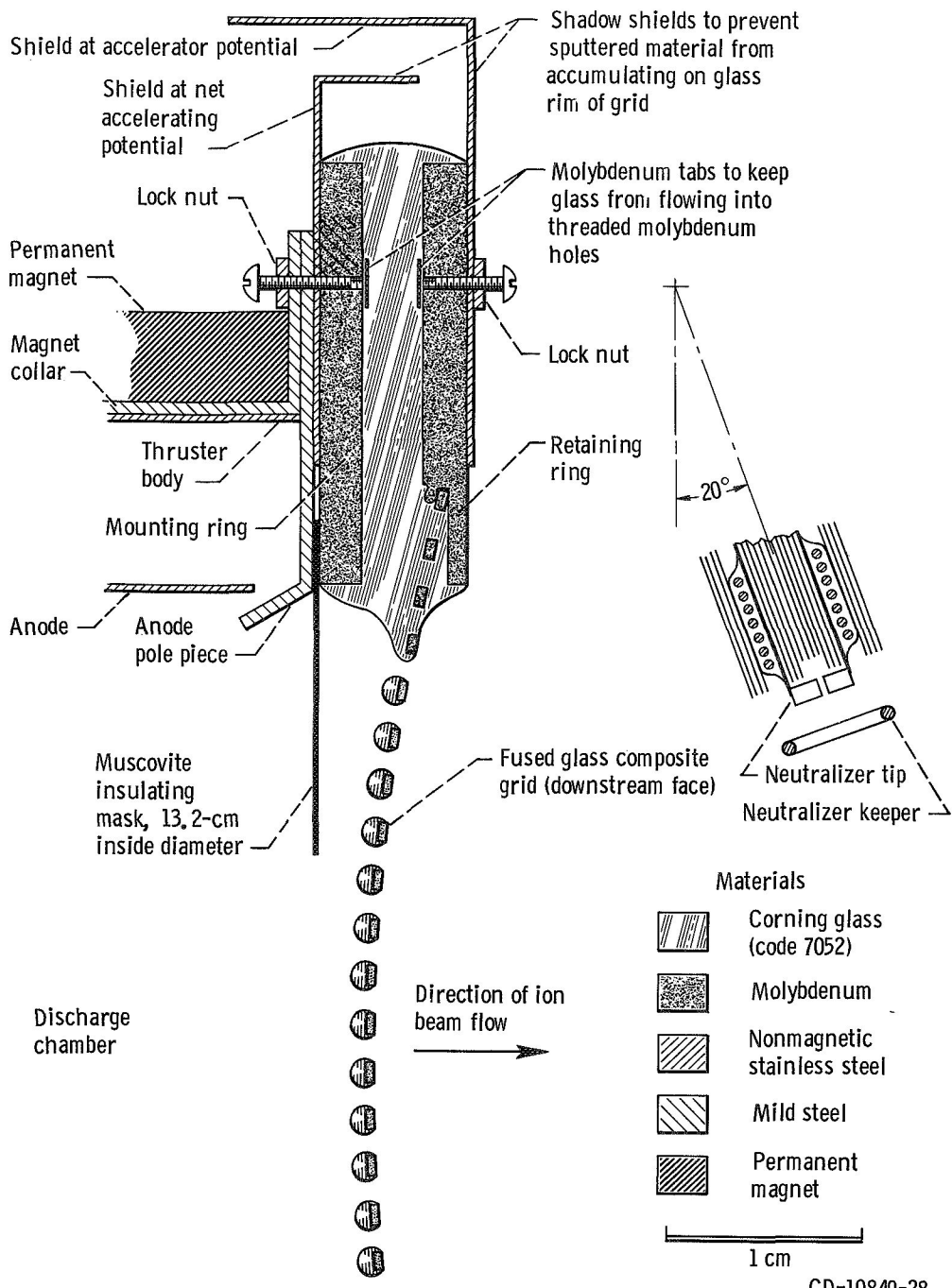
LAST 492 HOURS OF TEST - GRID-EDGE-TERMINATION STUDIES

After the 508-hour inspection of the grid, the test was resumed until a total of 557 hours of operation had accumulated on the grid. The run was halted at this time because of excessive arcing and high drain currents associated with the degraded grid-edge condition. Direct impingement of primary ions was occurring around the outer edge of the grid, where numerous breakdown sites had exposed the molybdenum part of the grid to the discharge chamber plasma. The accumulation of conducting sputtered material on the glass which insulates the grid mounting ring from the grid support ring also was permitting arcing to occur between the thruster body near V_I potential and the accelerator grid at V_A potential. Evidence of tracking due to arcing on the peripheral glass was also noticed.

An insulating annular mask consisting of muscovite mica flakes bound together with an inorganic binder was installed to shield the outer edge of the accelerator grid from the discharge plasma ions. This mask was 13.2 centimeters in inside diameter, 19.8 centimeters in outside diameter, and 0.813 millimeter thick. It was sandwiched between the shadow shield near V_I potential and the thruster anode pole piece (see fig. 14(a)). The grid was operated with this mask from run hour 557 to run hour 564, when it appeared that the downstream face of the mask was becoming coated with conducting sputtered material. This sputtered material was thought to be at or near the accelerator-grid potential V_A because of the conducting path along the sputtered material deposited on the glass beyond the outermost holes in the grid. Arcing and high drain currents were observed, probably from the discharge plasma shorting to the downstream face of the mask and along the sputtered glass surface to the accelerator grid.

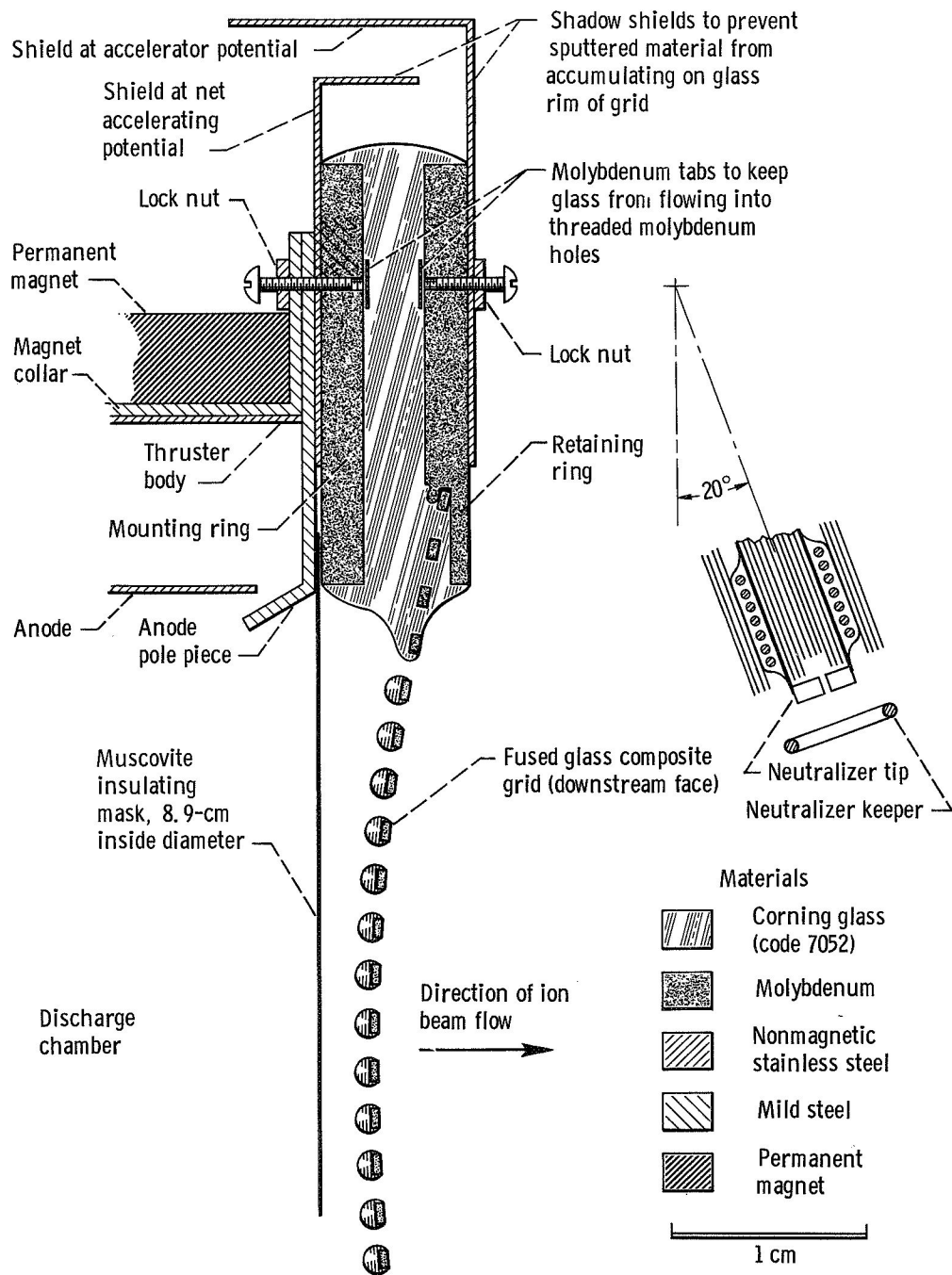
A wider insulating mask was then installed, as shown in figure 14(b). This mask was 8.9 centimeters in inside diameter, so that the distance from the inside diameter of the mask to the outermost hole region was 3.18 centimeters. This increased the distance required for sputtered material to provide a conduction path to the grid edge by a factor of 3, as compared to the mask shown in figure 14(a).

Because the effective grid extraction area was greatly reduced, the ion beam current was intentionally also reduced from 376 to 176 milliamperes. This was done to maintain an average ion beam current density which was more nearly equal to that during the first 508 hours of operation.



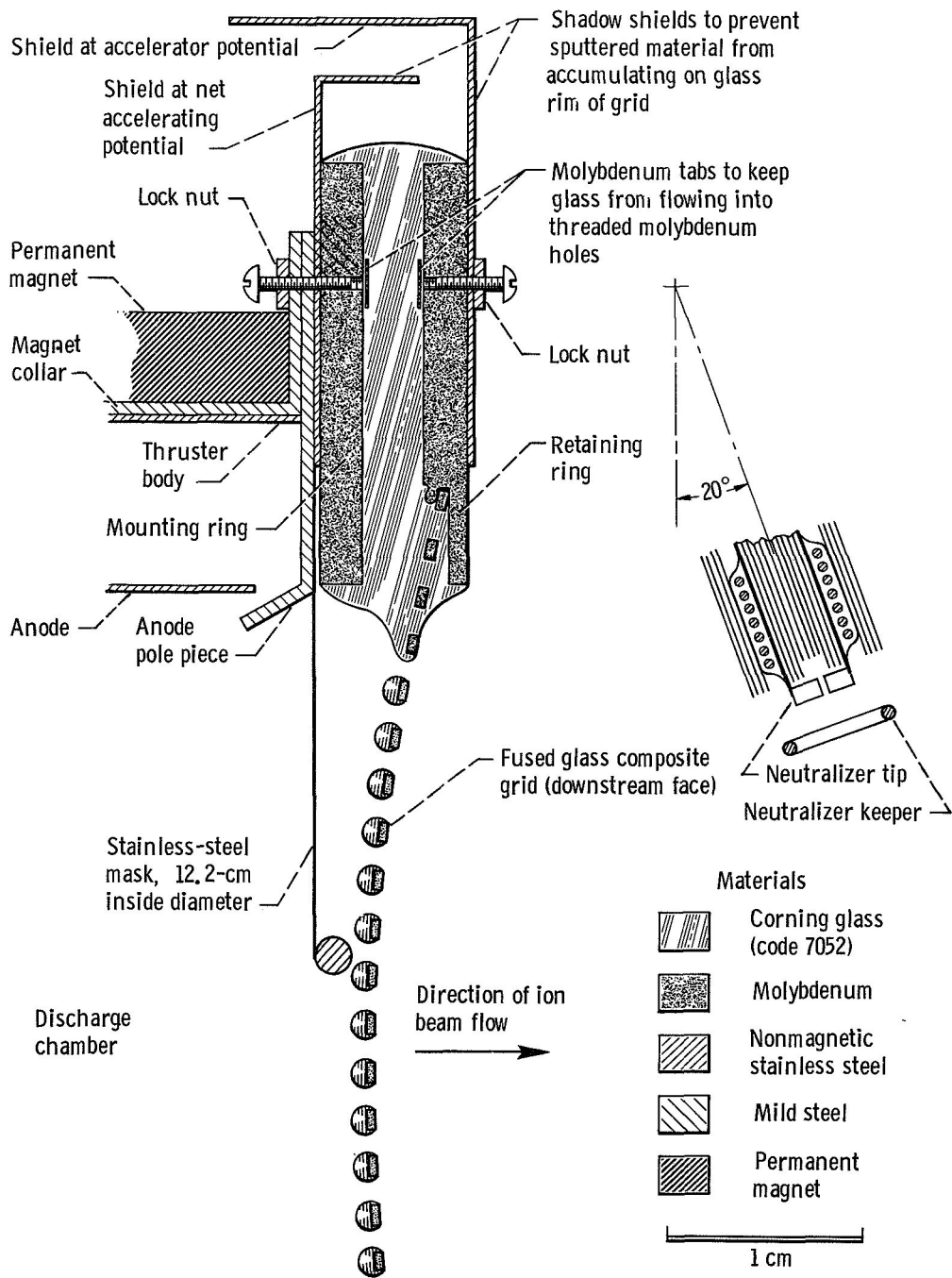
(a) 13.2-Centimeter-inside-diameter masked grid.

Figure 14. - Glass-coated grid-edge-termination geometries.



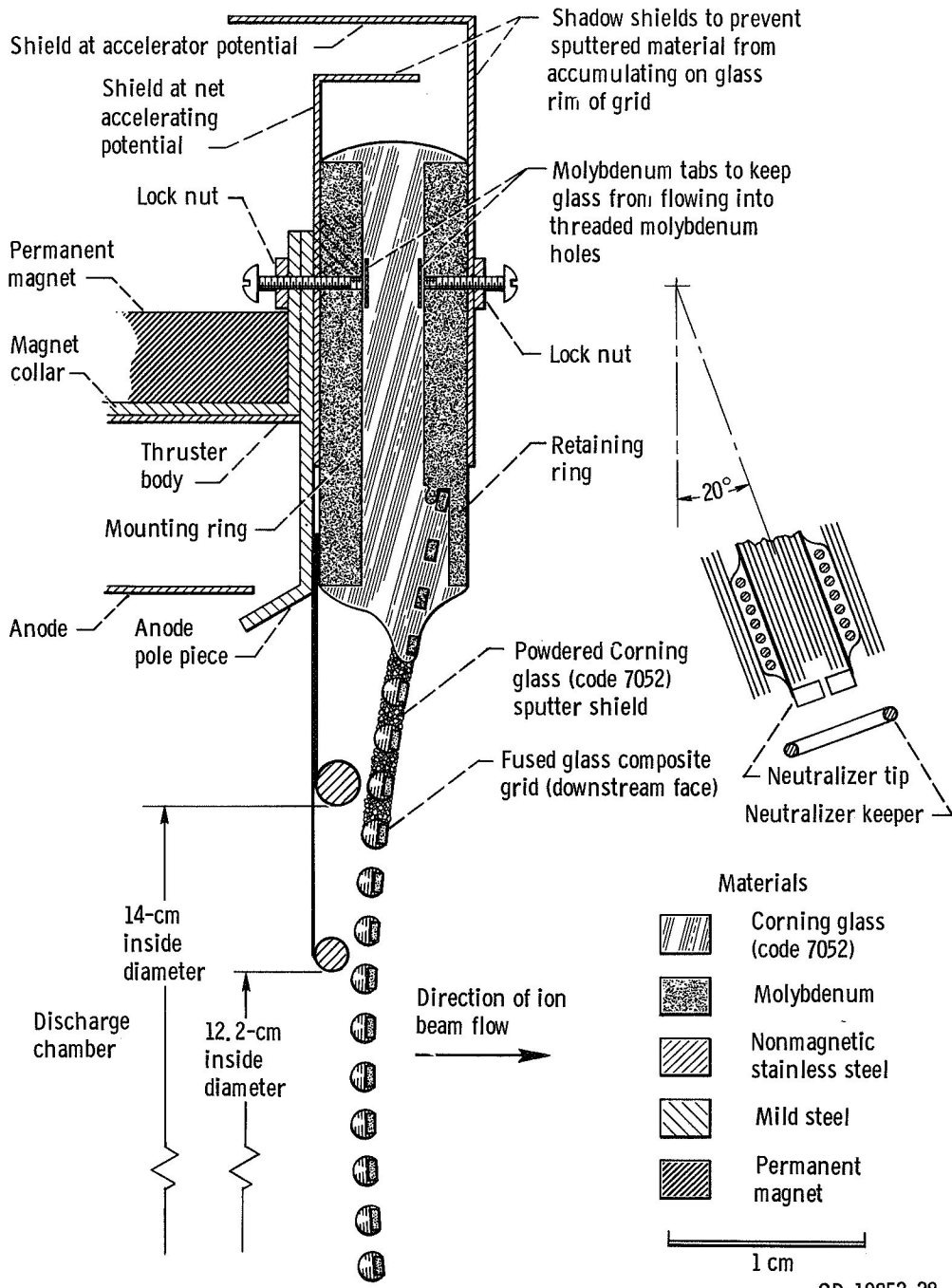
(b) 8.9-Centimeter-inside-diameter insulating masked grid.

Figure 14. - Continued.



(c) 12.2-centimeter-diameter single-metal-masked grid.

Figure 14. - Continued.



(d) Double-metal-masked grid with powdered Corning glass (code 7052) sputter shield.

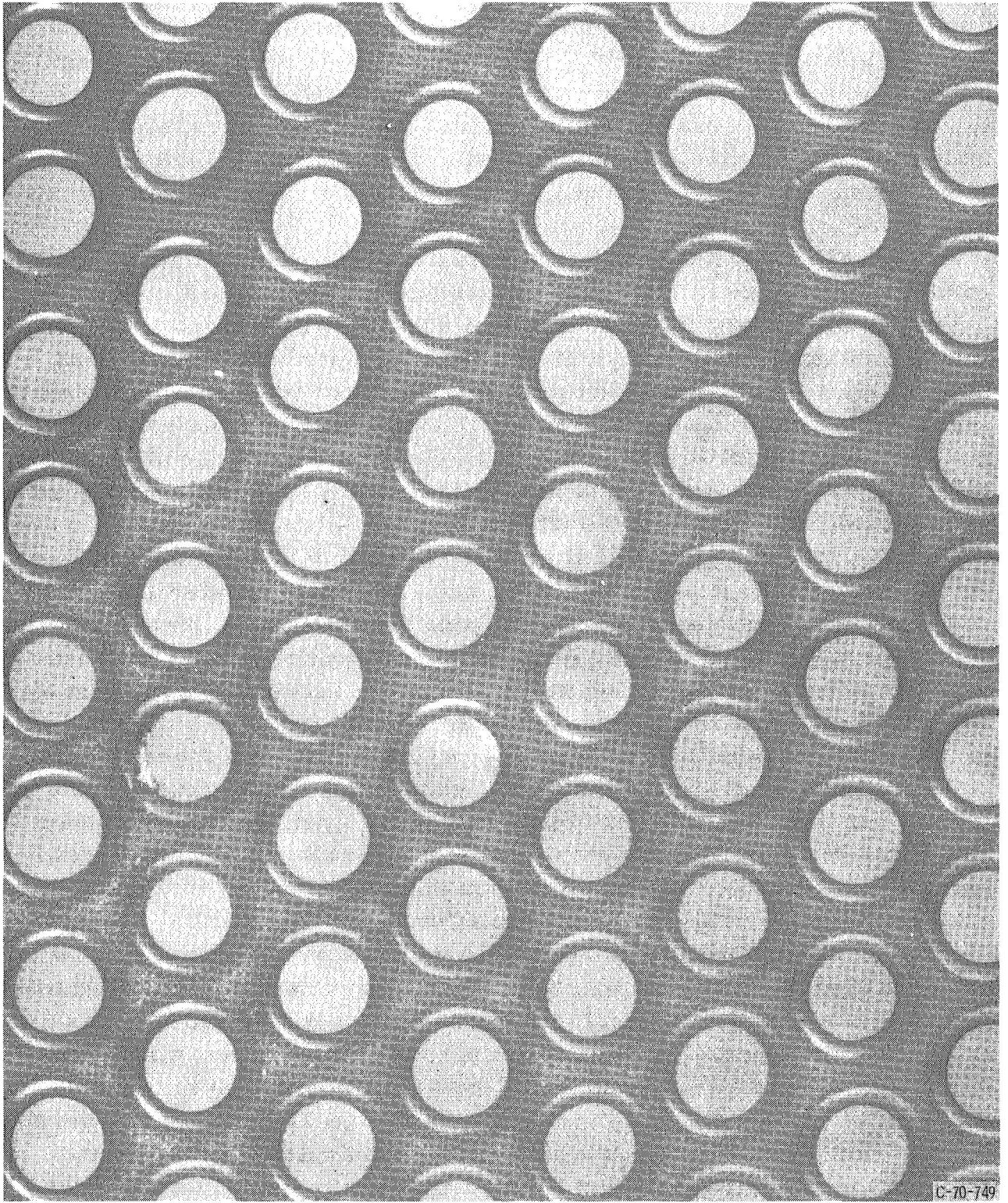
Figure 14. - Concluded.

During the interval that the grid was operated with this 8.9-centimeter-inside-diameter mask, a short test of the limit of high-voltage operation was also performed. A total voltage of over 2000 volts ($V_I + |V_A|$) was applied across the grid. Although no breakdown sites were produced, operation at higher total voltage was not possible because of momentary high drain currents to the V_I and V_A supplies. These spikes tended to trigger the automatic shutdown circuits in these supplies. A large percentage of the spikes coincided with observed sparking in the area of the innermost edge of the mask.

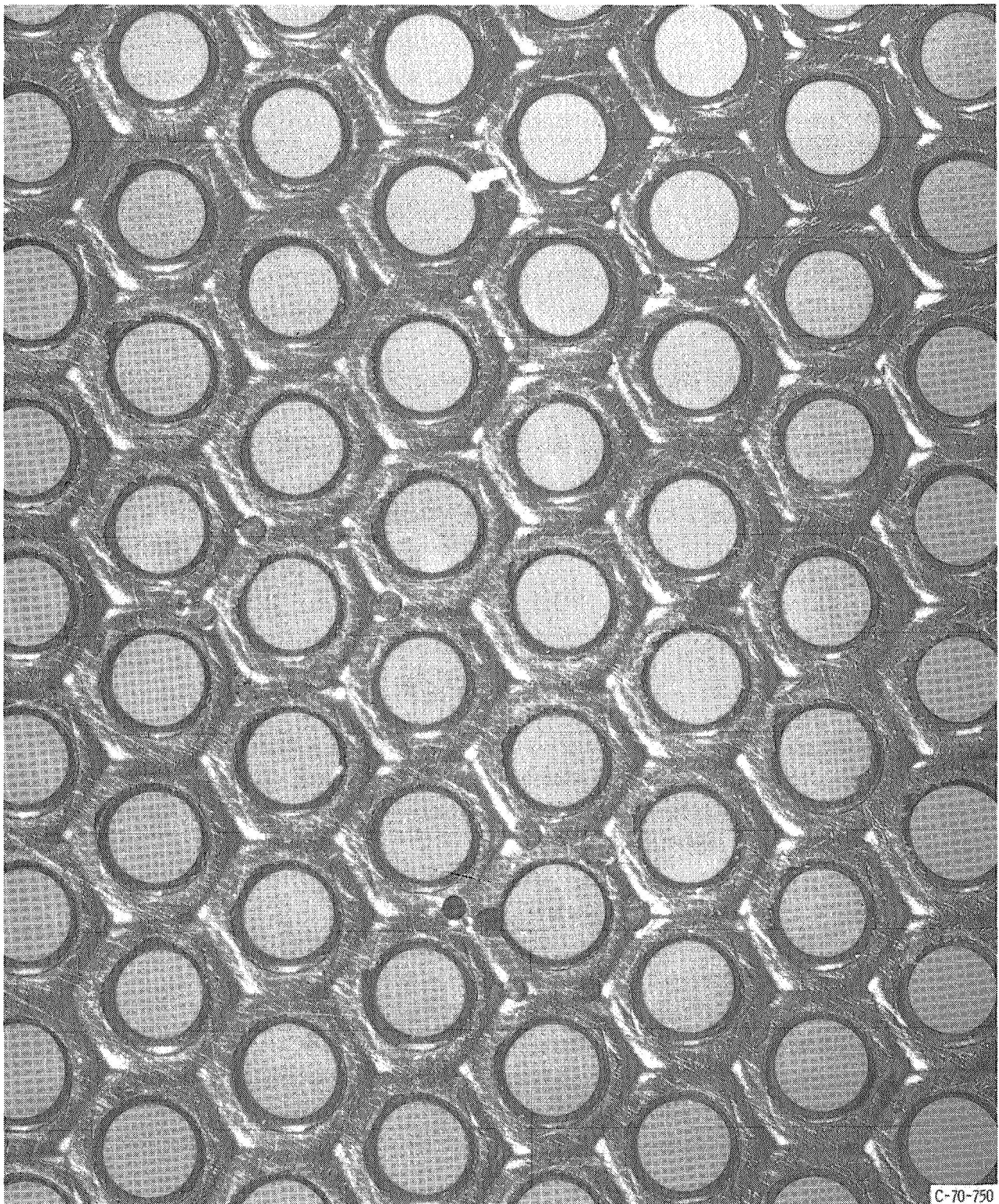
Thruster operation with the 8.9-centimeter mask was continued at the normal voltages until 804 hours operating time had been accumulated on the grid.

At this time a conducting mask, fabricated of 0.4-millimeter-thick type-304 stainless steel with an inside diameter of 12.2 centimeters, was completed. This mask, shown in figure 14(c), was designed to provide better shadow shielding and known potentials on the grid-edge-termination mask. This mask had a 1.59-centimeter-diameter type-304 stainless-steel wire spot-welded to the downstream inside edge to reduce the electric field concentrations. The purpose of the conducting mask was to provide known potentials and fields in the region between the mask and the accelerator grid. The ions which drifted into this region would have a high probability of being extracted because of the high electric fields in the gap between the metal mask near V_I potential and accelerator grid at V_A potential. Prior to grid operation with this mask, the inside surface of the glass separating the mounting ring from the grid retaining ring was sandblasted to remove all conducting sputtered material. Because this mask provided a larger effective grid ion extraction area than the previous insulating mask, the beam current was increased to approximately 375 milliamperes. Initial operation with this metal mask resulted in a low drain current of about 3.5 milliamperes (see fig. 8). However, after 38 hours with this metal mask (842-hr total grid running time), the accelerator drain current rose to over 20 milliamperes and remained high until the grid was removed at run hour 885. Resistance measurements indicated that sputtered material was again electrically shorting the mounting ring to the retaining ring.

It was apparent at this time that the accelerator drain current could be kept low only if the glass between the mounting ring and retaining ring was shadow shielded from the arrival of sputtered material. To accomplish this, the double metal mask shown in figure 14(d) was fabricated. The additional mask was 14.0 centimeters in inside diameter with a 0.238-centimeter-diameter wire (type-304 stainless steel) spot-welded to the downstream face of the mask. The glass surface between the mounting ring and the retaining ring was sandblasted until a negligible amount of conductivity was detected. A glass slurry was then prepared out of 325-mesh Corning glass (code 7052) and water. This slurry was applied to an annular region 1 centimeter wide around the periphery of the grid. Several applications were necessary before all the holes in this 1-centimeter-wide annulus were filled with powdered glass. This annulus was designed to provide



(a) Glass-coated upstream face of grid.
Figure 15. - Central area of glass-coated grid after 1000 hours of operation.



1 cm

(b) Uncoated downstream face of grid.

Figure 15. - Concluded.

shadow shielding for the glass at the edge of the grid. This combination of two metal masks and the dried glass slurry was found to provide adequate shadow shielding for the grid edge. The endurance test was resumed until 1000 total run hours had accumulated on the grid. The accelerator drain current during the final 115-hour grid test interval was less than 15 milliamperes, which indicated that shorting of the grid mounting ring to retaining ring did not occur.

The four different grid-edge-termination tests showed that adequate shadow shielding is essential to prevent sputtered material from shorting the accelerator grid (at V_A potential) to the grid mounting ring (near V_T potential). The best shadow shield was found to be one in which there was no line-of-sight path for sputtered material to reach the grid edge.

Although the grid was removed after 1000 hours of operation, there was no evidence of any problems that would prohibit further grid operation. Figures 15(a) and (b) show the coated and uncoated sides of the central area of the grid after 1000 hours of operation.

After the last 492 hours of operation, there was no observable increase in the erosion rate of the grid over that of the first 508 hours of operation, including that portion in the vicinity of the neutralizer.

SUMMARY OF RESULTS

The results of a 1000-hour endurance test of a glass (Corning 7052)-coated accelerator grid on a 15-centimeter-diameter Kaufman thruster are as follows:

1. The glass-coated grid was successfully operated for 508 hours at the following average operating conditions:

- a. 990 Volts net accelerating potential
- b. -456 Volts accelerator potential
- c. 373 Milliamperes mercury ion beam current
- d. 9.4 Milliamperes accelerator drain current
- e. Greater than 90 percent propellant utilization efficiency

2. The grid was inspected after the first 508 hours of operation and found to have numerous electrical breakdown sites in the glass coating near the outermost holes. This damage appeared to be caused by thin spots in the glass coating near these holes. The reduction in coating thickness was caused by the glass surface tension forces during firing.

3. There was no serious degradation in the central area of the grid. Predictions based on ion charge-exchange erosion of the downstream face of the grid in the central area indicate maximum grid lifetimes varying from 22 000 to 37 000 hours depending

on the assumed failure mode and providing that appropriate edge termination was provided.

4. Four grid-edge-termination configurations were tested during the last 492 hours of the 1000-hour endurance test. The tests indicated that the outer edge of the grid must be shadow shielded from the discharge plasma and from the arrival of sputtered material to ensure trouble-free operation of the grid. This was most nearly accomplished with the final grid design.

5. There was no observable neutralizer-related erosion of the grid after 1000 hours of operation.

6. The central area of the grid was free from breakdown sites or other forms of degradation at the conclusion of the test.

Lewis Research Center,
National Aeronautics and Space Administration,
Cleveland, Ohio, March 6, 1970,
120-26.

APPENDIX A

SYMBOLS

d	grid diameter, cm	J_V	main vaporizer current, A
F_m	grid fraction of metallic open area, dimensionless	k	Boltzmann constant, 1.38054×10^{-23} J/K
J_A	accelerator-grid drain current, A	L_g	glass-coating thickness, mm
J_B	ion beam current, A	T_g	glass temperature, K
J_E	emission current from cathode keeper system, A	T_{NV}	neutralizer vaporizer temperature, °C
J_I	anode current, A	V_A	accelerator-grid potential, V
J_{KK}	cathode keeper current, A	V_g	neutralizer floating potential, V
J_{KV}	cathode vaporizer current, A	V_I	net accelerating potential, V
J_{NE}	neutralizer emission current, A	ΔV_I	discharge potential, V
J_{NK}	neutralizer keeper current, A	ρ	resistivity of Corning glass (code 7052), Ω -m
J_{NV}	neutralizer vaporizer current, A		

APPENDIX B

EFFECT OF BREAKDOWN SITE LOCATION ON GRID DURABILITY

Electrical breakdown through the glass coating on a molybdenum accelerator grid results in exposure of the molybdenum grid to the plasma, which then causes direct ion impingement upon the molybdenum. This impingement will eventually sputter a hole through the molybdenum of approximately the same size as the initial breakdown site in the glass. Depending on the location of the initial breakdown site, the effect of the sputtering process may be either insignificant or catastrophic. Observations of numerous breakdown sites indicate that, if a site is located near a line of symmetry on the hexagonal hole array (see fig. 16), the erosion rate of the glass and metal will slow down once the molybdenum has a hole sputtered completely through it. Figures 17(a) to (c) show a typical breakdown site located near a symmetry line after 31, 47.75, and 78 hours of operation of a 5-centimeter-diameter grid. (Masking-tape rectangles were put on the grid, in some cases, to help locate the breakdown sites.) This grid had approximately the same glass-coating thickness, open area, and hole diameter as the grid discussed in the main text and was operated at an ion beam current of 32 milliamperes, a net accelerating potential of 400 volts, and an accelerator potential of -225 volts, on a 5-centimeter-diameter thruster.

If the breakdown site occurs off the lines of symmetry, direct ion impingement will continue to sputter molybdenum and glass, causing the breakdown site to enlarge as shown in figures 18(a) to (c). (These photographs were taken after 45.75, 52.5, and

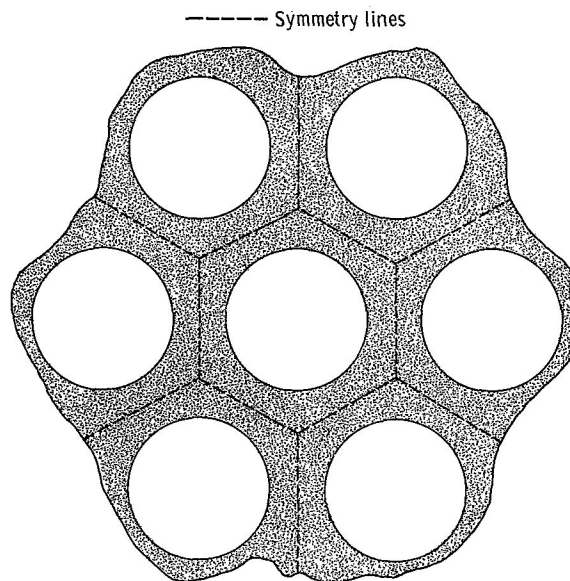
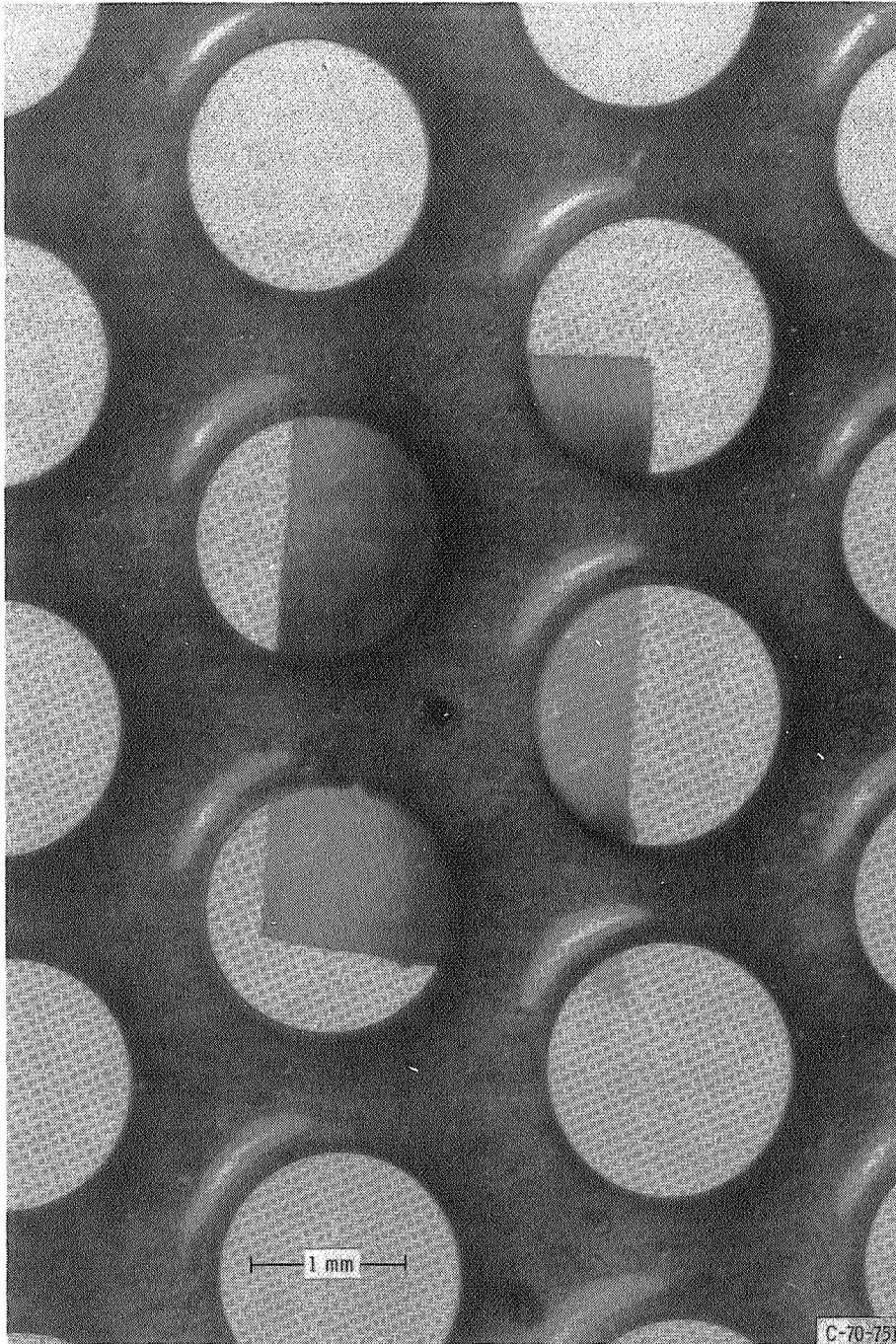
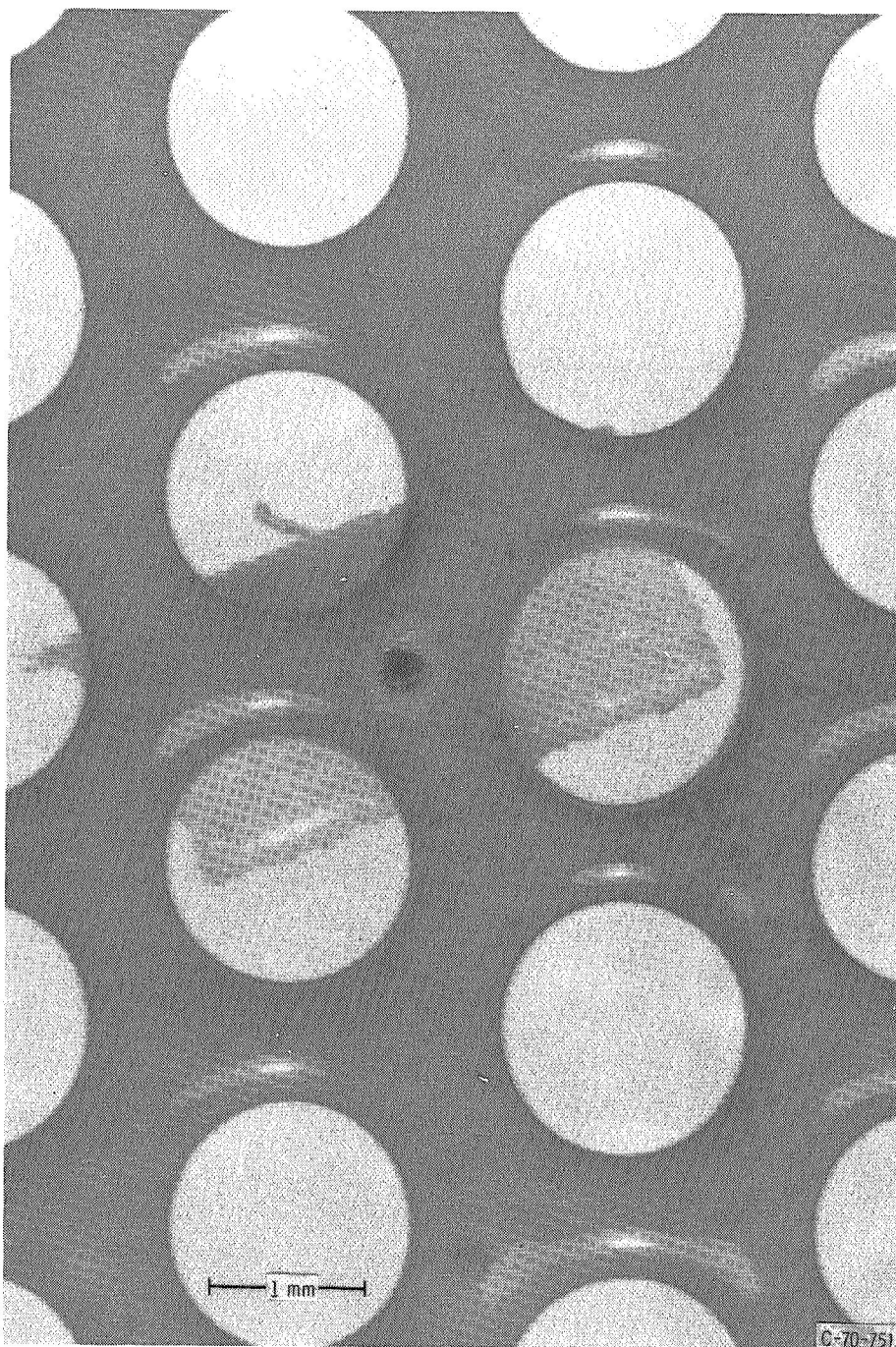


Figure 16. - Symmetry lines of a hexagonal hole array.

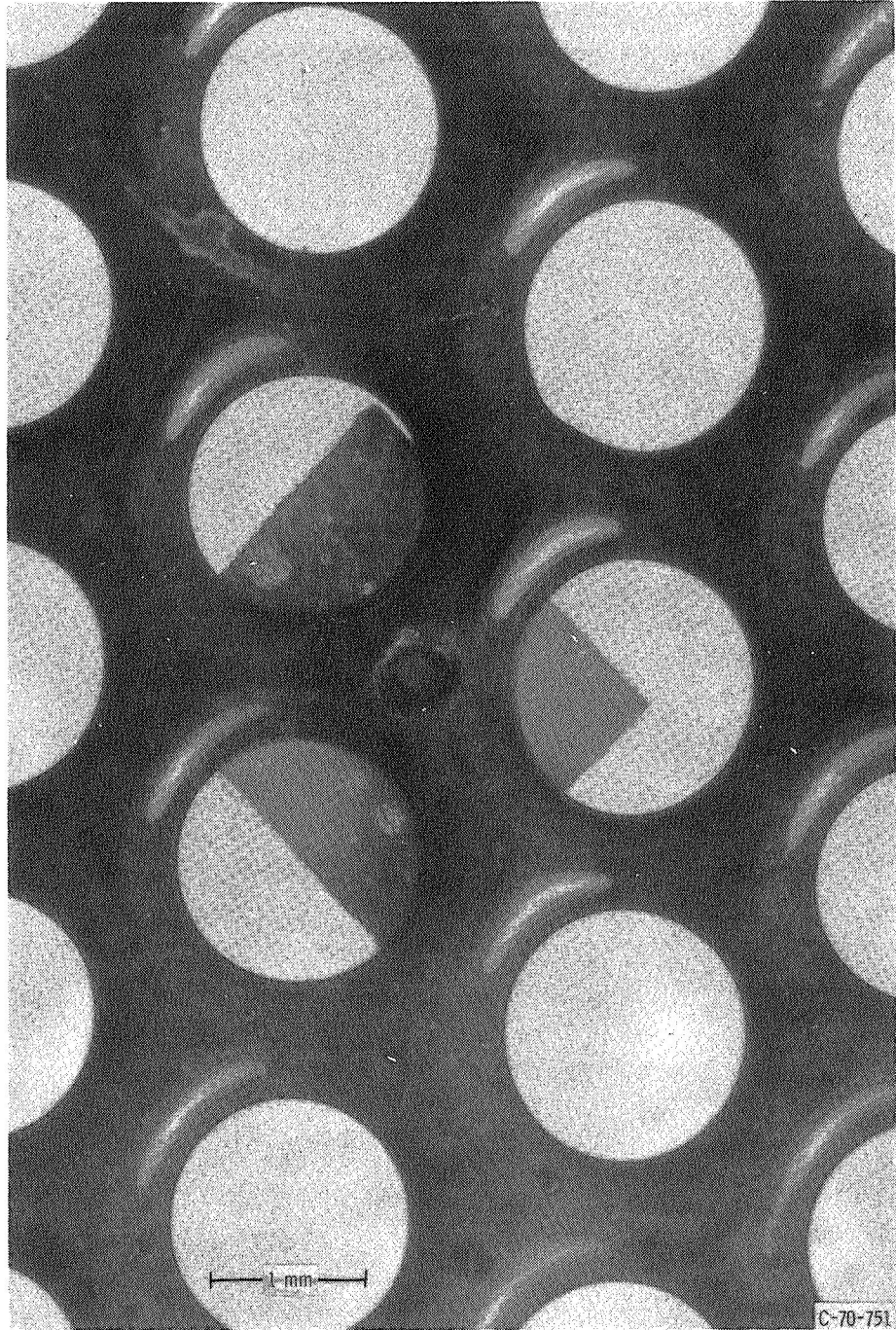


(a) After 31 hours of grid operation.

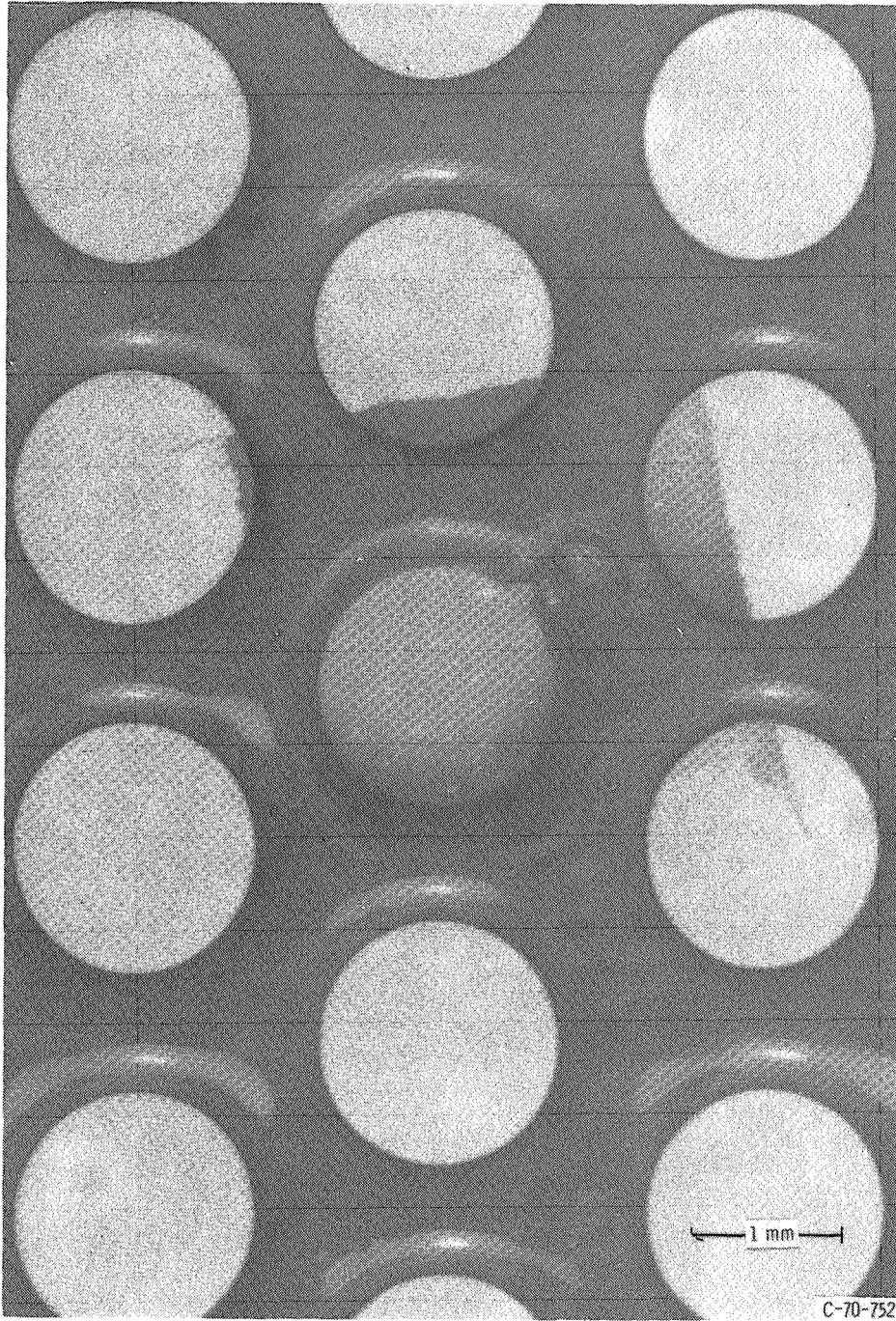
Figure 17. - Electrical breakdown site located near symmetry line in 5-centimeter-diameter grid.



(b) After 45.75 hours of grid operation.
Figure 17. - Continued.

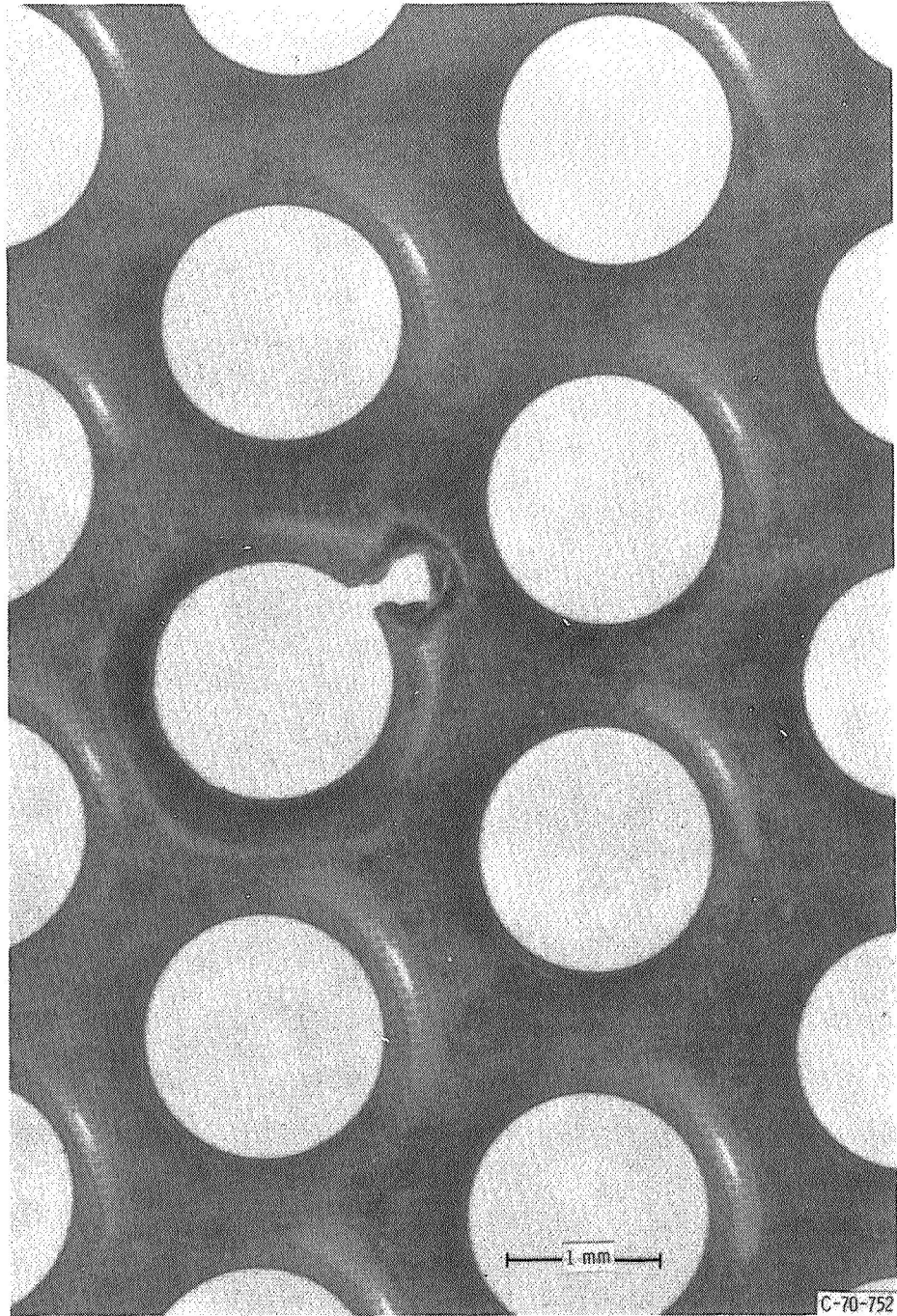


(c) After 78 hours of grid operation.
Figure 17. - Concluded.



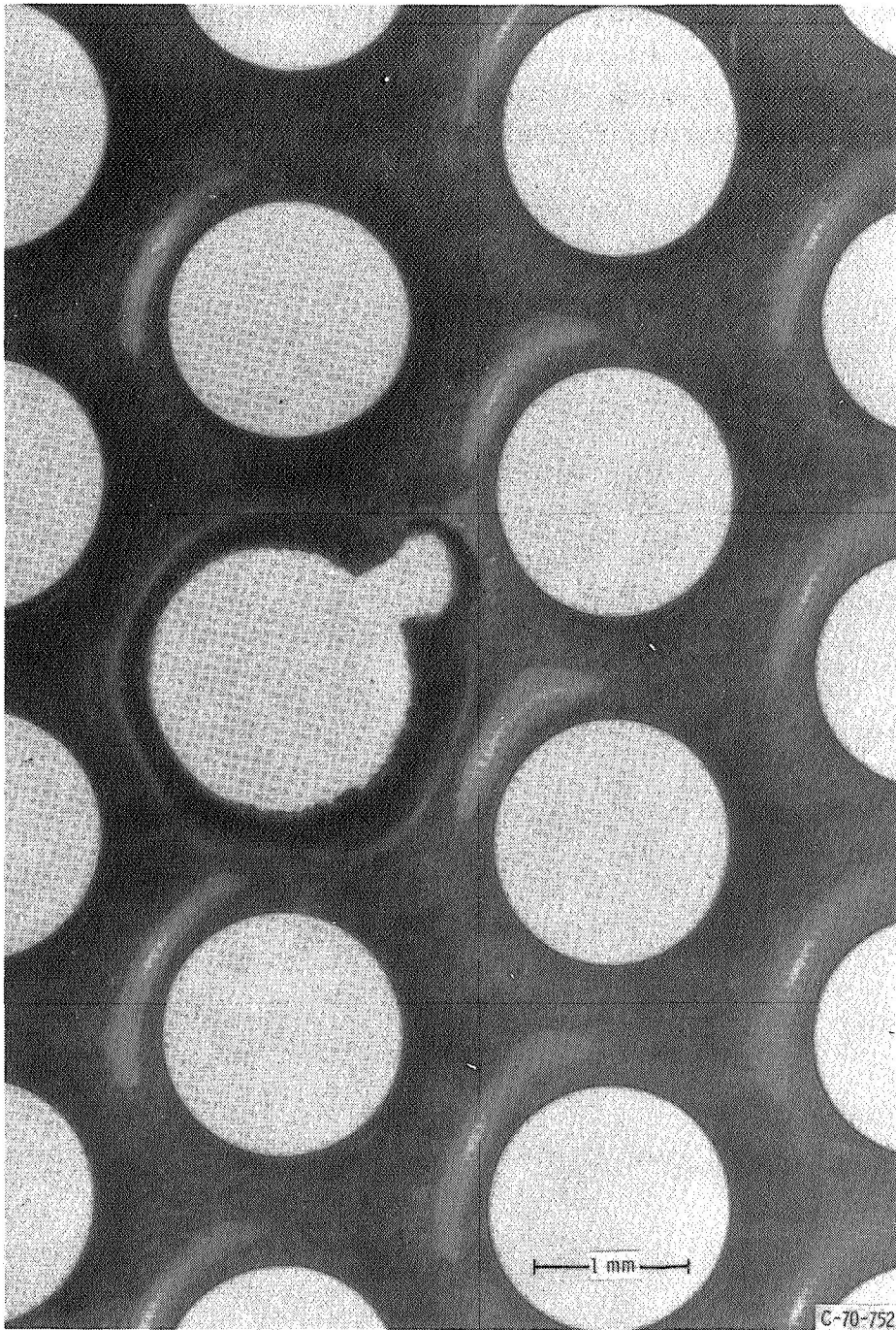
(a) After 45.75 hours of grid operation.

Figure 18. - Electrical breakdown site located far from symmetry line in 5-centimeter-diameter grid.



(b) After 52.5 hours of grid operation.

Figure 18. - Continued.



(c) After 78 hours of grid operation.
Figure 18. - Concluded.

78 hr operation.) As the metallic sputtered material collects on the glass hole walls that are still intact, it appears that direct ion impingement on the entire hole wall begins to occur. The result of this process is sputter erosion of the entire hole wall. Eventually, the glass and webbing surrounding the hole will completely erode, thus joining the initial breakdown site hole to another hole. This hole enlargement process continues and leads to eventual electron backstreaming when the hole becomes large enough.

REFERENCES

1. Margosian, Paul M.: Preliminary Tests of Insulated Accelerator Grid for Electron-Bombardment Thrusters. TM X-1342, 1967.
2. Nakanishi, S.; Richley, E. A.; and Banks, B. A.: High-Perveance Accelerator Grids for Low-Voltage Kaufman Thrusters. J. Spacecraft Rockets, vol. 5, no. 3, Mar. 1968, pp. 356-358.
3. Bechtel, Robert T.: Performance and Control of a 30-Centimeter Diameter, Low Impulse Kaufman Thruster. Paper 69-238, AIAA, Mar. 1969.
4. Banks, Bruce: Composite Ion Accelerator Grids. Paper presented at the Third International Conference on Electron and Ion Beam Science and Technology, Electrochemical Society, Boston, Mass., May 6-9, 1968.
5. Finke, Robert C.; Holmes, Arthur D.; and Keller, Thomas A.: Space Environment Facility for Electric Propulsion Systems Research. NASA TN D-2774, 1965.
6. Bechtel, R. T.; Csiky, G. A.; and Byers, D. C.: Performance of a 15-Centimeter Diameter, Hollow-Cathode Kaufman Thruster. Paper 68-88, AIAA, Jan. 1968.
7. Bechtel, Robert T.: Discharge Chamber Optimization of the SERT-II Thruster. J. Spacecraft Rockets, vol. 5, no. 7, July 1968, pp. 795-800.
8. Byers, David C.; and Staggs, John F.: SERT II Flight-Type Thruster System Performance. Paper 69-235, AIAA, Mar. 1969.
9. Banks, Bruce A.: A Fabrication Process for Glass Coated Electron-Bombardment Ion Thruster Grids. NASA TN D-5320, 1969.
10. Rawlin, V. K.; and Pawlik, E. V.: A Mercury Plasma-Bridge Neutralizer. J. Spacecraft Rockets, vol. 5, no. 7, July 1968, pp. 814-820.
11. Rawlin, Vincent K.; and Kerlake, William R.: Durability of the SERT II Hollow Cathode and Future Applications of Hollow Cathodes. Paper 69-304, AIAA, Mar. 1969.
12. Nichols, C. R.; and Obloy, S. J.: Automatic Controls for Facilities and Mercury Ion Thrusters in Durability Testing. J. Spacecraft Rockets, vol. 5, no. 12, Dec. 1968, pp. 1484-1486.

FIRST CLASS MAIL



POSTAGE AND FEES PAID
NATIONAL AERONAUTICS
SPACE ADMINISTRATION

POSTMASTER: If Undeliverable (Section 1103, Postal Manual) Do Not Return

"The aeronautical and space activities of the United States shall be conducted so as to contribute . . . to the expansion of human knowledge of phenomena in the atmosphere and space. The Administration shall provide for the widest practicable and appropriate dissemination of information concerning its activities and the results thereof."

— NATIONAL AERONAUTICS AND SPACE ACT OF 1958

NASA SCIENTIFIC AND TECHNICAL PUBLICATIONS

TECHNICAL REPORTS: Scientific and technical information considered important, complete, and a lasting contribution to existing knowledge.

TECHNICAL NOTES: Information less broad in scope but nevertheless of importance as a contribution to existing knowledge.

TECHNICAL MEMORANDUMS: Information receiving limited distribution because of preliminary data, security classification, or other reasons.

CONTRACTOR REPORTS: Scientific and technical information generated under a NASA contract or grant and considered an important contribution to existing knowledge.

TECHNICAL TRANSLATIONS: Information published in a foreign language considered to merit NASA distribution in English.

SPECIAL PUBLICATIONS: Information derived from or of value to NASA activities. Publications include conference proceedings, monographs, data compilations, handbooks, sourcebooks, and special bibliographies.

TECHNOLOGY UTILIZATION PUBLICATIONS: Information on technology used by NASA that may be of particular interest in commercial and other non-aerospace applications. Publications include Tech Briefs, Technology Utilization Reports and Notes, and Technology Surveys.

Details on the availability of these publications may be obtained from:

**SCIENTIFIC AND TECHNICAL INFORMATION DIVISION
NATIONAL AERONAUTICS AND SPACE ADMINISTRATION
Washington, D.C. 20546**